Title: H2A.Z and elongation factor Spt6 form an ancient bridge shaping transcription in eukaryotes

Authors: Zachary H. Harvey,[1,*] Kathryn M. Stevens,[2,3] Tobias Warnecke,[2,3,4,**] Frédéric Berger[1,***]

Affiliations:

[1]Gregor Mendel Institute, Austrian Academy of Sciences, Vienna, Austria

[2]MRC Laboratory of Medical Sciences, London, United Kingdom

[3]Institute of Clinical Sciences, Imperial College London, London, United Kingdom

[4]Trinity College, Oxford, United Kingdom

*Correspondence: zachary.harvey@gmi.oeaw.ac.at

**Correspondence: tobias.warnecke@lms.mrc.ac.uk

***Correspondence: frederic.berger@gmi.oeaw.ac.at

SUMMARY

Since eukaryogenesis, chromatin has evolved to regulate gene expression. The histone variant H2A.Z is an ancestral, essential feature of eukaryotic chromatin linked to transcription. Curiously, it is a transcriptional activator in some species and a repressor in others, suggesting species-specific differences shape its function. Here we engineer H2A.Z sequence variants from diverse eukaryotes into a single host, *Schizosaccharomyces pombe*, to understand H2A.Z's transcriptional impact. We show that H2A.Z sequences representing more than a billion years of evolution encode functional variation attributable to as little as single amino acid substitutions in the unstructured loop 2 (L2) region of H2A.Z's core domain. We show that L2 binds elongation factor Spt6, with L2 sequence influencing its binding to Spt6 and whether it promotes or restricts transcription elongation. In this way, the H2A.Z-Spt6 interaction clarifies H2A.Z's fundamental regulatory function, providing a direct physical and functional linkage between transcription and its chromatinized template across eukaryotes.

INTRODUCTION

Eukaryotic RNA polymerase II (RNAPII) transcribes mRNA from DNA that is organized into repeating units of ~147 bp of DNA wrapped around a multi-subunit protein complex, the nucleosome.[1] Over the past fifty years, an enormous body of work has established the importance of nucleosomes in regulating transcription[2-7] in development,[8] disease,[9] and in response to stress.[10] The prevailing model is that nucleosomes are obstacles to transcription initiation, and that chromatin remodeling (moving or removing nucleosomes) is required to enable the first steps of gene expression.[11-20] This model centers on the first nucleosome of the transcriptional unit positioned adjacent to the transcription start site, which is known to be critical for transcription initiation.[21-23] However, there is a clear linkage between the degree to which a gene is expressed and its nucleosome composition throughout the transcriptional unit,[24-26] suggesting that nucleosomes throughout the gene body likely also contribute to transcriptional output.

One of the most prominent features of nucleosome composition is the frequent presence of a histone H2A variant, H2A.Z.[4,27-32] First discovered nearly 45 years ago,[33,34] genes encoding H2A.Z have been identified in divergent eukaryotes, suggesting that it might be an ancient paralog, dating back to the last eukaryotic common ancestor.[35] H2A.Z is essential in many species,[36-38] reduces nucleosome stability both *in vitro*[39,40] and *in vivo*,[41,42] and has been linked to transcription.[43-47] Yet, precisely how H2A.Z affects the activity of RNAPII is unclear.

Studies of various model organisms have yielded apparently conflicting conclusions. For example, whereas works in *Tetrahymena*, *Drosophila*, and budding yeast suggested that H2A.Z has an activating role in transcription,[2,3,27,33,41,46,48] other studies—in fission yeast, plants, human cells, and *in vitro*—have supported a repressive role.[28,47,49-53] Whether these divergent findings might be explained by species-specific differences in the primary sequence of H2A.Z has not been established.

Here, we use phylogenetic analysis and a synthetic approach to identify a direct molecular link between H2A.Z and the transcription machinery, establishing its fundamental mode of action and rationalizing its variable, species-specific impact on transcription. We evaluate the impact of H2A.Z sequence variation representing more than a billion years of eukaryotic evolution in a single experimentally tractable synthetic system, the fission yeast *Schizosaccharomyces pombe*, replacing the endogenous *S. pombe* H2A.Z (Pht1) with H2A.Z sequences from diverse eukaryotes. We identify the transcription elongation factor Spt6 as a direct physical interactor of the loop 2 (L2) region of the H2A.Z core domain. Finally, we establish that even single amino acid differences in the L2 region impact transcription at the level of elongation. Together, our findings indicate that an ancient interaction between H2A.Z and Spt6 connects RNAPII directly to the chromatin template, providing insight into its fundamental role in eukaryotic gene expression.

RESULTS

H2A.Z is an ancient histone variant

To test our hypothesis that species-specific differences in the primary sequence of H2A.Z might explain their differences in function, we first identified H2A proteins from diverse eukaryotes in the EukProt database (Figures 1, S1 and S2A; Supplementary Table S1; Supplementary Data File 1; Methods). We used the sequences of these H2A proteins to build phylogenetic trees from which we could investigate the evolutionary history of H2A.Z in the context of other H2A histones. As previously suggested from analyses of smaller datasets,[35,54] we found that H2A.Z forms a monophyletic clade that spans nearly the entirety of known eukaryotic diversity (Figure 1A, Figure S2B). Almost all sequences in this clade, but very few outside of it, harbor the signature DEELD motif located in a C-terminal region of H2A.Zs referred to as the docking domain (DD).[35] A small cluster of sequences, mostly from the

unicellular flagellate *Carpediemonas membranifera* (phylum Metamonada), branch just outside the H2A.Z clade, contain a near-perfect, but nevertheless variable, DEELD motif and might represent rare, divergent forms of H2A.Z (Figure S2B). Other H2A variants either have a more restricted phylogenetic distribution (e.g. macroH2A and H2A.W) or cannot be traced to a single ancestral sequence, appearing paraphyletic (e.g. H2A.X) (Figure 1A and 1B). Importantly, we found H2A.Z orthologs in nearly every eukaryotic genome, even in deep-branching clades like Metamonada that were previously thought to lack H2A.Z[55] (Figure S2B). Thus, the phylogenetic distribution points to H2A.Z being present in the last eukaryotic common ancestor (LECA), and broadly retained throughout the evolution of eukaryotes. These findings support the view that H2A.Z is the only H2A variant whose ancestry can be traced back to the LECA.

Phylogenetically diverse H2A.Z sequences drive distinct gain-of-function transcriptional states

To investigate how sequence divergence affects H2A.Z function, we selected nine H2A.Z sequences from across the phylogenetic tree (Figures S2B and S3A, Supplementary Data File S2). The sequences were selected to maximize the number of eukaryotic supergroups represented, and their total sequence diversity. Although they span more than a billion years of evolution, these representative H2A.Z proteins were ~65–90% identical in their core domain (excluding highly divergent N- and C-terminal tail regions; Figure S3B), highlighting their high degree of conservation.

To test whether transcription is impacted by sequence diversity in these nine representative H2A.Z proteins, we synthesized *S. pombe* codon-optimized versions of the nine H2A.Z ortholog coding sequences, and generated yeast lines in which the endogenous gene encoding H2A.Z (*pht1*) was replaced by one of these orthologs (Figure 2A). We then assessed

whether these replacement lines phenocopied the wild-type (WT) gene, resembled a H2A.Z deletion mutant (*pht1*$^{-}$), or differed from both.

We assessed global transcriptional changes in the replacement lines by using strand-specific mRNA-seq. Consistent with prior reports,[2] *pht1*$^{-}$ cells exhibited modest transcriptional changes, affecting ~10% of detected transcripts (Figure S3C). By contrast, many H2A.Z replacement lines showed changes in ≥20% of detected transcripts when compared with WT (Figure S3C). To investigate this further, we examined how similar the transcriptomes of the nine H2A.Z replacement lines were to either WT or *pht1*$^{-}$ using principal component analysis. Replacement lines differed markedly both from WT and *pht1*$^{-}$ (Figure 2B), suggesting that H2A.Zs from different species are not simply gradations of total loss of function alleles, but give rise to sequence-specific gain-of-function states.

We next asked whether transcriptional variation in H2A.Z from different species had consequence at the level of phenotype. To do this, we assessed the growth of H2A.Z replacement lines using a plate-based assay in the presence of stress conditions targeting metabolism (rapamycin[56]), protein folding (low-dose guanidinium hydrochloride[57]), cell wall biogenesis (clotrimazole[58]), fermentation (ethanol[59]), or either directly (doxorubicin[60], formamide[61]) or indirectly (caffeine[62]) transcription and chromatin (Figure 2C). Consistent with functional variation at the level of transcriptomes, the growth of all nine replacement lines differed substantially from WT and *pht1*$^{-}$ cells across all tested conditions (Figure 2C), with most lines growing more slowly than *pht1*$^{-}$ cells. Notably, greater sequence divergence of replacement orthologs from *S. pombe* Pht1 correlated with weaker growth in several stress conditions, with the strongest correlation being for conditions known to be linked directly to transcription (doxorubicin, formamide) or stresses known to require a transcriptional response (ethanol[59]) (Figure 2D, Figure S3D). By contrast, we saw no strong correlation between the level of H2A.Z expression and growth (Figure 2D, Figure S3D), indicating that these effects

were not attributable to differential expression of H2A.Z but likely related to differences in the primary sequence. Together, these data link primary sequence variation in H2A.Z from different species to variation in its function and confirm a tight linkage between H2A.Z and transcription.

The L2 region of H2A.Z is a key determinant of its function

Histone proteins are composed of a core histone-fold domain, characterized by a nearly sequence-invariant bundle of three alpha helices ($\alpha 1, \alpha 2,$ and $\alpha 3$), bounded by mostly unstructured N- and C-terminal tails and separated by two unstructured loop regions, L1 and L2 (Figure 3A).[1] To pinpoint which sequence domains of H2A.Z are responsible for changes in transcriptional output across the set of orthologs tested above, we first examined sequence conservation across the full H2A.Z dataset (Figure 1), calculating sequence identity along the length of H2A.Z using a 3-residue sliding window average (Figure 3A). As expected, we observed high conservation of the core alpha-helical bundle and relatively lower conservation of the tails and the L1 (Figure 3A). Surprisingly, however, we found that parts of the L2 region, specifically around the core motif KDLKVK, were as highly conserved as the core α-helices (Figure 3A). This was especially striking when compared with the H2A variant H2A.X, which was notably less conserved in this region.

The unexpectedly high sequence conservation of the L2 region suggested it might play a role in determining the global changes in transcription we observed in the replacement *S. pombe* lines. To test this, we engineered a series of chimeric histone genes whereby the N, C, L1, L2, or docking domain[35] (DD) regions of *S. pombe pht1* were substituted into histone H2A (*hta1*) (Figure 3B, Figure S4A). We expressed each of these chimeric genes by knocking them into the *pht1* locus and assayed their ability to complement the *pht1*$^{-}$ null allele by measuring the growth of the chimeric lines under selected stress conditions based on prior experiments

with the representative full-length H2A.Z replacement lines (Figure 2). The chimeric histone genes fell into two groups across all phenotypes tested: those that partially complemented the *pht1*$^{-}$ mutant (those encoding H2A/Z^{DD}, H2A/Z^{N}, and H2A/Z^{L1}) and those that fully complemented the *pht1*$^{-}$ mutant in all tested conditions (those encoding H2A/Z^{L2} and H2A/Z^{C}), making them indistinguishable from WT (Figure 3C). These data indicate that both the L2 region and the C-terminal tail play key roles in determining H2A.Z function.

To investigate whether sequence variation in the L2 region of H2A.Z alone is sufficient to explain the transcriptional differences we observed in our full-length H2A.Z replacement lines, we looked for a correlation between transcriptional divergence and sequence divergence from WT *S. pombe* in any of the structurally defined primary sequence regions of H2A.Z. Although the short L2 affords limited resolution, we observed a strong correlation between L2 sequence divergence and transcriptional divergence ($\rho = 0.63$, $p < 10^{-3}$, Figure 3D). By contrast, the sequence divergence of the C-terminal tail, which fully complemented the *pht1*$^{-}$ mutant in growth assays, did not correlate with transcriptional divergence ($\rho = 0.056$, $p = 0.8$, Figure 3D). There was also a correlation between the sequence divergence of the N-terminal tail and transcriptional divergence ($\rho = 0.5$, $p < 10^{-2}$; Figure S4B). This was likely due to co-variation with the L2 sequence, as there was a tight correlation between sequence variation in these two regions ($\rho = 0.77$, $p < 10^{-5}$, Figure S4B) and the N-terminal tail chimera, H2A/Z^{N}, did not strongly complement *pht1*$^{-}$. Together, these data show that the L2 region of H2A.Z is an important contributor to its function.

The L2 region of H2A.Z binds to transcription elongation factor Spt6

The L2 region of H2A.Z is largely solvent accessible,[63] particularly during transcription when the DNA is unwrapped from the nucleosome.[64,65] We therefore hypothesized that L2 might alter transcription by physically interacting with proteins involved in transcription, rather

than by influencing histone–DNA contacts, as is the case for the L2 region of histone H3.[1,66] To identify proteins in the *S. pombe* nuclear proteome that might interact with the L2 region of Pht1, we used AlphaFold2 Multimer[67] to predict physical interactions. We first performed a virtual interaction screen of WT Pht1 L2 against the *S. pombe* annotated proteome[68,69] (Figure 4A), identifying 247 proteins with an interface predicted template modelling (IPTM) score threshold of >0.5 (Supplementary Table S2). To further refine potential interactors, we reasoned that L2 interactors responsible for driving functional variation in transcriptional output must vary in their interaction in accordance with their L2 primary sequence. We thus selected 17 unique single-residue variants of the L2 core motif from our database of H2A.Z sequences (Figure 1, Supplementary Data File S1), performing an AlphaFold2 virtual interaction screen with correspondingly mutated Pht1 L2 sequences against a subset of 500 nuclear proteins based on their IPTM score with WT Pht1 L2 (Figure 4B, Figure S5A, Supplementary Table S3). To assess differences in predicted binding across Pht1 mutants, we then calculated the variance in IPTM score for each candidate interactor protein (Figure 4C). In most cases, the variance was very low, suggesting that the candidate interacting proteins do not respond to variation in L2 (Figure 4C, Figure S5A, Supplementary Table S3). Among the candidate interactors with the highest variance, the transcription elongation factor Spt6 (Figure 4D and 4E, Supplementary Table S3) was the only component of RNAPII.[70,71] It interacts with nucleosomes,[72-74] had highly robust folding models across multiple simulations (Figure S5B), and closely matched experimentally derived structures (Figure S5C).

We first experimentally validated the AlphaFold2-predicted interaction between Pht1 and Spt6, using glutathione-S-transferase (GST) as negative control. H2A was previously reported to bind to Spt6 and was used as positive control.[75] We expressed and purified recombinant *S. pombe* GST-tagged Pht1 and Hta1, and His-tagged Spt6 in *Escherichia coli* (Figure 4F) and assessed binding *in vitro* to nickel resin (binds the His tag). Pht1 bound Spt6

(Figure 4G), confirming the Pht1–Spt6 interaction. Further, we noted a qualitative difference in the amount of Hta1 and Pht1 bound to Spt6, suggesting that the two histone proteins might interact differently with Spt6. To verify this finding, we repeated Spt6-Pht1 pulldown experiments under more stringent binding conditions, where the amount of bound Pht1 was considerably less than that of Hta1 (Figure S5D), reinforcing the suggestion Hta1 and Pht1 may interact with Spt6 differently. Together, these data establish a physical interaction between Spt6 and Pht1.

To test whether the L2 region was sufficient to mediate the Pht1–Spt6 interaction, we synthesized a biotinylated peptide corresponding to this region of *S. pombe* Pht1 and assayed its binding to His-tagged Spt6 (Figure 4H). As a negative control, we used a peptide corresponding to the docking domain (DD) of *S. pombe* Pht1, which is adjacent to the L2 region and important for the interaction of Pht1 with H3 and H4[63] and Swr1-C.[76] Whereas the DD peptide did not bind Spt6, the peptides corresponding to the L2 region of Hta1 or Pht1 bound Spt6 (Figure 4I), consistent with the results of our experiments with the full-length proteins. These data establish that the L2 region alone is sufficient to explain the interaction of Pht1 with Spt6.

To test whether sequence variation in the L2 region of H2A.Z alters its binding to Spt6, we synthesized L2 peptides from five of the original set of representative H2A.Z sequences and assayed their binding to *S. pombe* Spt6, as above. Consistent with the sequence of L2 determining its interaction with Spt6, we observed variable amount of each peptide bound to Spt6 across species (Figure 4I), with *A. godoyi*, *T. globosa*, and *P. marinus* H2A.Z L2 peptides having the greatest qualitative difference relative to *S. pombe* Pht1 L2. Although there were clear differences between peptides derived from different species, we did not observe a strong association between Spt6-binding and sequence similarity (Figure 4I), suggesting that specific sequence features of the peptides, rather than overall sequence divergence, must govern their

association with Spt6. Indeed, when we compared the sequence of the three species' L2 peptides that had discernable differences relative to Pht1 to those that did not, we noted that all of them had substitutions within the L2 core motif (Figure S5F), especially at position L83.

To investigate the role of sequence variation in the core motif around L83 in determining the binding of Pht1 L2 to Spt6, we further examined AlphaFold2 models. Pht1 is predicted to bind to the Spt6 death-like domain (DLD) (Figure 4D). This domain, whose function has remained uncharacterized, is the most highly conserved feature of the Spt6 surface,[77] suggesting an important functional role. To assess this further, we gathered Spt6 sequences from the same EukProt database we used previously to identify H2A.Zs, calculating sequence conservation of the DLD across known eukaryotic diversity (Figure 4J). When we examined the amino acid composition of the DLD, we noted large numbers of hydrophobic residues that were not only highly conserved in absolute terms (Figure 4J), but also relative to other hydrophobic residues in Spt6 ($p < 0.005$, Wilcoxon test; Figure S5F). These residues were organized into a hydrophobic groove, many of which contacted the Pht1 L2 core motif in AlphaFold2 models (Figure 4E, Figure S5E). Further, these contacts were predicted to vary according to the H2A.Z L2 sequence, both when examining models for L2s from different species (Figure S5E), as well as Pht1 mutants to the L83 position we identified earlier (Figure 4E), suggesting a rationale for why sequence variation at this Pht1 position might affect binding.

To test the contribution of Pht1 L2 sequence variation, particularly at position L83, to the Pht1–Spt6 interaction in the context of the DLD hydrophobic groove, we synthesized three mutated Pht1 L2 peptides with either more hydrophobic (L83F) or more hydrophilic (L83M, L83N) substitutions and tested their binding to Spt6. Whereas L83F mutant L2 peptide bound Spt6 similarly to WT Pht1 peptide, Spt6 bound both more hydrophilic substitutions (L83M/N) to a much lesser extent than WT Pht1 L2 (Figure 4I). These relative binding abilities

corresponded to their hydrophobicities, and are thus consistent with AlphaFold2 predictions that the L2 region of Pht1 interacts with the hydrophobic groove of the DLD of Spt6 (Figure 4D). Notably, although L83 is important for the Pht1–Spt6 interaction, the more hydrophilic L83N substitution, which corresponds to Hta1 residue N75, does not recapitulate the binding of full-length Hta1 (Figure 4D), reinforcing our earlier conclusion that numerous other primary sequences differences in Hta1 (Figure S4A) must contribute to its binding. Together, these findings suggest that the hydrophobic L2 region of H2A.Z determines its binding to the DLD of Spt6.

H2A.Z L2 regulates transcription elongation

Since Spt6 is a transcription elongation factor,[70,71] we hypothesized that sequence variation in the L2 region of H2A.Z might be sufficient to affect transcription elongation, thereby explaining species-specific differences in reported H2A.Z function. To test this, we first developed a growth-based reporter assay using the uracil biosynthesis gene *ura4*. In this assay, the amount of transcription of *ura4* is directly related to the amount of growth in media lacking uracil (Figure 5A). Assaying a growth-based reporter has the advantage that it can be used to test multiple conditions and it is not easily confounded by global transcriptional changes. We first confirmed that our reporter gene accumulates Pht1 by ChIP-qPCR (Figure S6A). We then introduced point mutations corresponding to those found in the L2 core motif of our nine representative H2A.Z orthologs (Figures S3A and S5F) into the endogenous *pht1* (H2A.Z) gene in *S. pombe* (Figure 5B). Whereas *pht1*$^{-}$ cells gave rise to a modest increase in reporter expression (Figure 5C), supporting a repressive function of H2A.Z in *S. pombe* as in some other model systems,[47,49,50,53] half of L2 mutants had a significant increase (by ~1.3–1.5 fold for L83F, L83N and L83Q) or decrease (by ~2 fold for L83M) in reporter expression. These results were not confounded by general fitness defects in the mutant strains (Figure

S6B), and all the mutants were epistatic to Swc2, an essential subunit of the Swr1-C chromatin remodeling complex, which incorporates H2A.Z into nucleosomes[78,79] (Figure S6C). Together these results establish that reporter expression differences are driven by Pht1 presence at the reporter gene and suggest that L2 sequence variation is sufficient to impact transcription.

We next tested whether differences in reporter expression across Pht1 mutant lines were specifically attributable to transcription elongation through two orthogonal approaches. First, focusing on the four Pht1 mutant lines with the strongest differences in reporter expression relative to WT (L83M, L83N, K86Q, and L83F), we made use of the drug mycophenolic acid (MPA) to specifically interfere with RNAPII elongation by lowering cellular GTP levels.[80] In this experiment, if a mutant has increased or decreased RNAPII elongation relative to WT, then it should be resistant or sensitive to MPA, respectively. Treatment of WT cells with MPA caused a ~40% reduction in growth relative to the control (Figure 5D). By contrast, *pht1*$^{-}$ and the Pht1 mutants L83N, K86Q, and L83F, which all have relatively high levels of transcription, were more resistant to MPA than the WT (~25–35% reduction in growth; Figure 5D), consistent with increased transcription elongation in these lines. By contrast, the single mutant that had decreased reporter expression (L83M) was also the most sensitive to MPA treatment (~60% reduction, $p_{adj} < 10^{6}$, Figure 5D), confirming its reduction in transcription elongation activity. Together, these data establish that Pht1 L2 mutants are sufficient to impact elongating RNAPII.

Finally, as an orthogonal measure to our reporter-based assays, we probed the impact of Pht1 L2 mutants on transcription elongation by measuring nascent transcription using precision run-on sequencing (qPRO-seq).[81,82] Sequencing nascent transcripts allowed us to position RNAPII in the transcriptional unit and to distinguish between promoter-proximal paused RNAPII and gene body-located RNAPII participating in active elongation across all expressed genes, albeit without accurately quantifying specific parameters of RNAPII activity. Consistent

with results of our reporter assays, differential expression analysis of gene body-located qPRO-seq counts in the WT and *pht1*$^{-}$ lines showed a modest increase in active elongation by RNAPII at ~100 genes in *pht1*$^{-}$ cells (Figure 5E). Similar analyses of the Pht1 point mutant lines identified three classes of mutant. In one class, comprising half of the tested mutants (L83M, L83G, A80S, and V85A), we observed essentially no change in RNAPII elongation, when compared with WT at the level of differentially transcribed genes (Figure 5E). Notably, this class included the single super-repressive L2 mutant (L83M). Since it was also the sole Pht1 mutant that maintained a mild transcriptional phenotype in a *swc2*$^{-}$ background (Fig. S6C), it may have acquired an additional interaction driving its function. The second class comprised a single mutant (K84H), which had a modest increase in RNAPII engaging in elongation, very similar to that of *pht1*$^{-}$ (Figure 5E). The third class comprised three mutants (L83N, K86Q, and L83F) in which we observed a robust increase in RNAPII engaging in elongation at ~50% more genes than in *pht1*$^{-}$ (Figure 5E), consistent with their impact on reporter gene transcription. Together, these data establish that sequence variation in the L2 region is sufficient to explain species-specific effects of the presence of H2A.Z in gene bodies on transcription.

DISCUSSION

We set out to understand why H2A.Z function diverges across eukaryotes—why it activates transcription in some species and represses it in others. In *S. pombe*, as in plants and mammalian cells,[49,50] H2A.Z (Pht1) is generally antagonistic towards transcription elongation. We show here that H2A.Z basic activity can be modified by sequence variations as small as single point mutations in the L2 core motif, which through their physical interaction with Spt6 give rise to changes in transcriptional output. In this way, although H2A.Z itself is deeply conserved across species, it is likely that its specific qualitative role in transcription regulation––i.e. activation, repression—is not. Rather, we propose the conserved and core function of H2A.Z across eukaryotes is its very potential to regulate RNAPII via Spt6. In this way, H2A.Z helps build the 'ground state' of transcription. Its presence (or absence) within nucleosomes specifies the chromatin template's inherent potential to be efficiently transcribed by RNAPII, communicating through the Spt6 subunit. This ground state might be refined and sculpted by chromatin remodelers and modifiers to achieve context-specific gene expression, setting the stage for dynamic modes of transcription regulation—e.g. transcription factors. That small sequence variants can become rapidly amplified, resetting the ground state of transcription genome wide accounts for the observation that H2A.Z has both species- and locus-specific complexity.

We establish that H2A.Z L2 binds Spt6, which allosterically regulates RNAPII[83] to impact transcription elongation.[70,71] To date, work seeking to address a potential link between Spt6 and chromatin has focused on its chaperone-like functions in maintaining chromatin structure during transcription,[72,73,75] yet Spt6 contains several functional domains.[77] We suggest that the DLD of Spt6 is a key driver of its function in shaping transcription[73,75] as it directly interacts with H2A.Z and this is sufficient to change the rate of elongation by RNAPII. In this way, our findings highlight the inherent complexity of RNAPII, pointing to a need to

understand how the often parallel, yet still interdependent, functions of transcription are orchestrated in time and space.

How the interaction between H2A.Z and Spt6 mechanistically influences the function of RNAPII remains a question for future studies. One mechanism, however, might be by inducing conformational changes in RNAPII. Conformational changes to negative elongation factor (NELF) were recently demonstrated to control the transition of RNAPII from paused to poised for transcription by allosterically changing the active site of RNAPII to a more permissive state.[84] Structural work will establish if H2A.Z–Spt6 uses a similar mechanism and whether this explains why even single change of amino acids participating in this interaction induce strong changes in transcription. If so, this might explain why cross-species comparisons of even highly conserved proteins often yield inconclusive models of exact molecular function if small, perhaps overlooked, changes in primary sequence are amplified by allosteric protein–protein interactions.

For much of the past 50 years, investigations into variation in the core histone fold have focused on its interaction with DNA and, in particular, the fact that H2A variants impact the stability of the nucleosome.[39-41,85-89] Our findings, by contrast, highlight the importance of the histone core domain for genomic regulation through protein–protein interactions, corroborating similar recent reports,[66,90,91] identifying a mechanism based on the interaction of H2A.Z and the Spt6 DLD that, due to the ubiquity of these two proteins across the eukaryotic tree of life, likely originated with the birth of eukaryotes. That we uncover sequence variation in just seven residues of the L2 core motif of H2A.Z can give rise to enormous phenotypic complexity at the level of transcriptional output and the H2A.Z–Spt6 interaction, it is plausible that many protein–protein interactions with the nucleosome core domain remain to be discovered. Indeed, given the extreme depth of conservation of not only H2A.Z and Spt6, but also the entire chromatin and transcription apparatus across eukaryotic evolution, [92] it seems

likely that the nucleosome core is the center of a rich and extensive world of chromatin regulation.

Limitations of the study

A key limitation of this study is that we have not studied the roles of H2A.Z orthologs in the various species in which they were identified. This poses a formidable technical challenge given the lack of experimental tractability of non-model species, particularly those harboring H2A.Z sequence variants with the greatest impact on transcriptional output. Also, we do not take into account any mechanisms that might compensate for functional defects in H2A.Z orthologs expressed in *S. pombe*. This might be a fruitful avenue to discover potentially new mechanisms regulating histone and chromatin biology.

ACKNOWLEDGEMENTS

We thank the entire Berger group and Antoine Hocher, for their insightful, considerate, and helpful discussions, as well as Carol Featherstone from Life Science Editors and Matt Watson for editorial assistance during the preparation of the manuscript. We especially thank Zdravko Lorković, Elin Axelsson-Ekker, and Chung Hyun Cho for their invaluable assistance preparing antibodies, biochemical assays, and bioinformatic analyses. We also thank John T. Lis for advice with qPRO-seq. This work was supported by grants to FB and ZHH from the Österreichischer Wissenschaftsfonds FWF (TAI304, ESP213, respectively), as well as core funding from the Austrian Academy of Sciences (ÖAW) to FB. ZHH was further funded by an EMBO Postdoctoral Fellowship (ALTF169-2020). Work in the Warnecke lab is supported by core funding from United Kingdom Research and Innovation's Medical Research Council (MC_A658_5TY40). We thank the Molecular Biology Service and Media Kitchen for a constant supply of plates, basic reagents, and cloning and sequencing services, as well as the Peptide Synthesis Service. Additionally, we thank the Vienna BioCenter Core Facilities, in particular the Next Generation Sequencing facility for their advice and swift handling of all our requests and the Protein Technologies facility for their expertise, helpful discussions, and recombinant protein production.

AUTHOR CONTRIBUTIONS

Conceptualization: ZHH, FB, and TW; Methodology: ZHH, KS, and TW; Validation: ZHH and KS; Formal Analysis: ZHH, KS, and TW; Investigation: ZHH, KS, and TW; Data Curation: ZHH, KS, and TW; Writing – original draft: ZHH, TW, and FB; Visualization: ZHH, KS, and TW; Supervision: FB, TW; Project Administration: ZHH; Funding Acquisition: ZHH, FB, and TW.

DECLARATIONS OF INTEREST

Z.H.H. and F.B. are inventors on a patent submitted by the Gregor Mendel Institute at the Austrian Patent Office (A50392/2024) pertaining to the modification of transcription and fitness by engineering H2A.Z L2.

FIGURES AND FIGURE LEGENDS

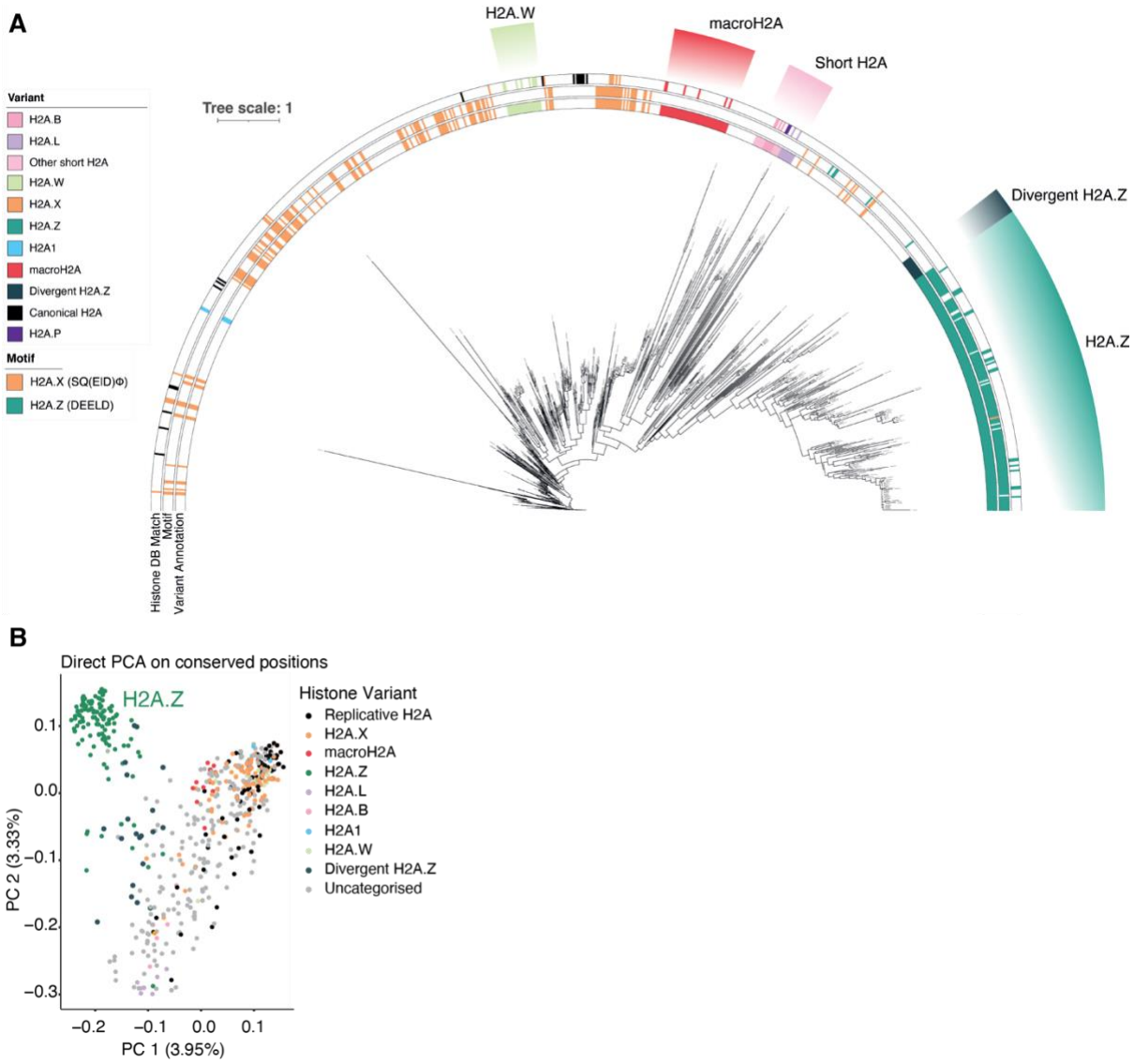
A
H2A.W
macroH2A
Short H2A
Tree scale: 1
Variant
H2A.B
H2A.L
Other short H2A
H2A.W
H2A.X
H2A.Z
H2A1
macroH2A
Divergent H2A.Z
Canonical H2A
H2A.P
Motif
H2A.X (SQ(EID)Φ)
H2A.Z (DEELD)
Divergent H2A.Z
H2A.Z
Histone DB Match
Motif
Variant Annotation
B
Direct PCA on conserved positions
H2A.Z
Histone Variant
Replicative H2A
H2A.X
macroH2A
H2A.Z
H2A.L
H2A.B
H2A1
H2A.W
Divergent H2A.Z
Uncategorised
PC 2 (3.33%)
PC 1 (3.95%)
0.1
0.0
−0.1
−0.2
−0.3
−0.2
−0.1
0.0
0.1

Figure 1. H2A.Z is an ancient histone variant. A, Unrooted protein phylogeny of H2A (see Methods for reconstruction details). H2A.Z, as defined by the presence of a 'DEELD' motif within its docking domain, are colored in green. 'Divergent' H2A.Zs branch as a sister to the major H2A.Z clade and carry at least one substitution in the DEELD motif. **B**, Principal component analysis (PCA) on H2A sequences displayed in A, annotated by variant identity.

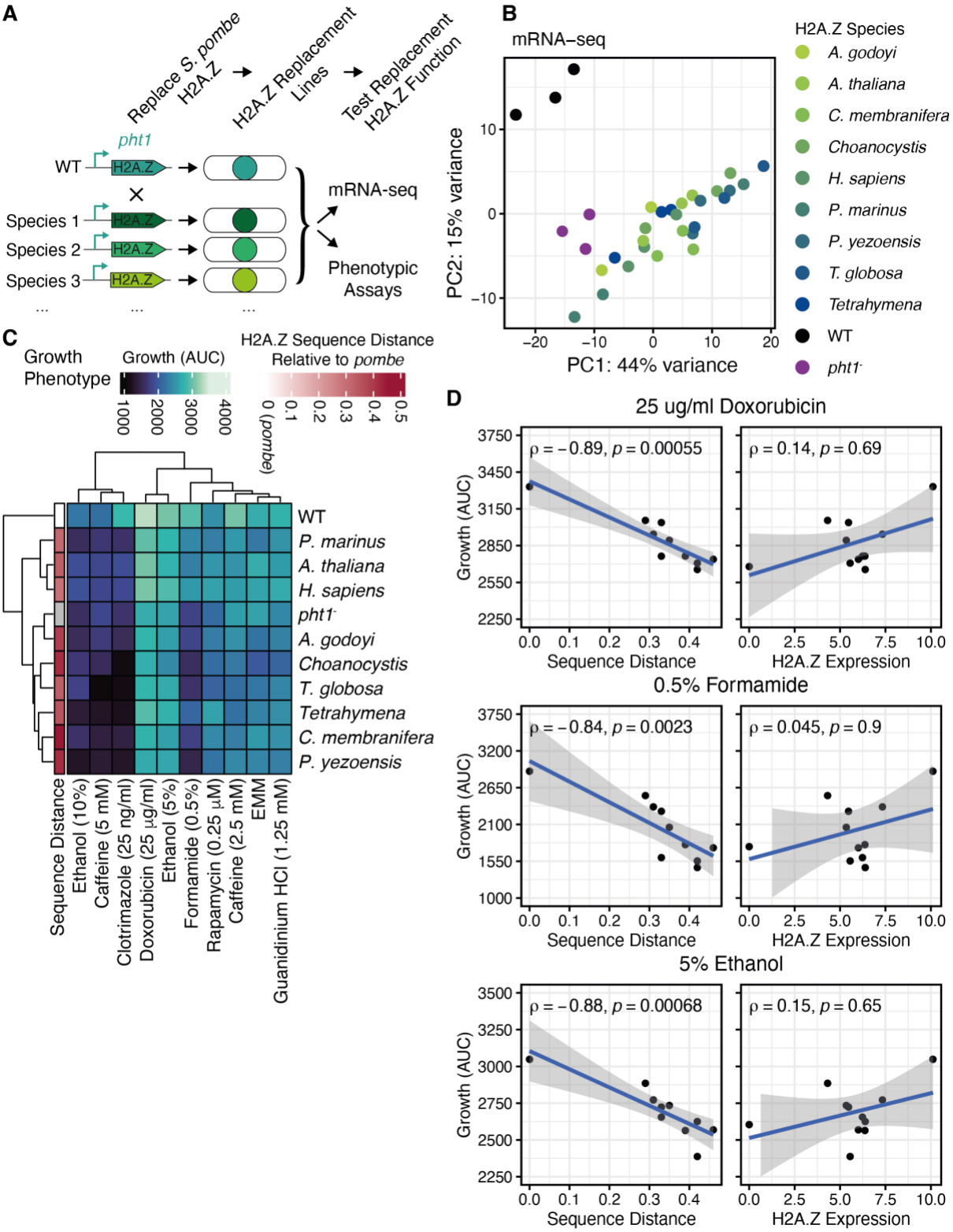
A
Replace S. pombe H2A.Z
H2A.Z Replacement Lines
Test Replacement H2A.Z Function
pht1
WT
H2A.Z
Species 1
Species 2
Species 3
mRNA-seq
Phenotypic Assays
B
mRNA–seq
PC2: 15% variance
PC1: 44% variance
H2A.Z Species
A. godoyi
A. thaliana
C. membranifera
Choanocystis
H. sapiens
P. marinus
P. yezoensis
T. globosa
Tetrahymena
WT
pht1-
C
Growth Phenotype
Growth (AUC)
H2A.Z Sequence Distance Relative to pombe
Sequence Distance
Ethanol (10%)
Caffeine (5 mM)
Clotrimazole (25 ng/ml)
Doxorubicin (25 μg/ml)
Ethanol (5%)
Formamide (0.5%)
Rapamycin (0.25 μM)
Caffeine (2.5 mM)
EMM
Guanidinium HCl (1.25 mM)
D
25 ug/ml Doxorubicin
ρ = −0.89, p = 0.00055
ρ = 0.14, p = 0.69
0.5% Formamide
ρ = −0.84, p = 0.0023
ρ = 0.045, p = 0.9
5% Ethanol
ρ = −0.88, p = 0.00068
ρ = 0.15, p = 0.65
Growth (AUC)
Sequence Distance
H2A.Z Expression

420

421

Figure 2. Phylogenetically diverse H2A.Z sequences drive distinct gain-of-function transcriptional states. A, Experimental scheme describing the replacement of endogenous *S. pombe pht1* by representative H2A.Zs taken from the H2A phylogeny (Figures 1A and S2B). **B**, Principal component analysis (PCA) for the top 500 variable genes from mRNA-seq data generated for H2A.Z replacement lines. **C**, Growth phenotypes for H2A.Z replacement lines in various stress conditions, annotated with the sequence distance of each H2A.Z from that of *S. pombe* Pht1 (which has a sequence distance of zero). Plotted values are the mean of four biological replicates. Growth is quantified as the area under the curve (AUC) from respective growth curves. H2A.Zs are annotated with their sequence distance relative to *S. pombe* Pht1, with zero being Pht1 and larger numbers indicating greater divergence. **D**, Example Spearman's correlations between the growth from (C) with either sequence distance (as in C) of each H2A.Z relative to WT *S. pombe*, or the expression of the respective H2A.Z (from mRNA-seq).

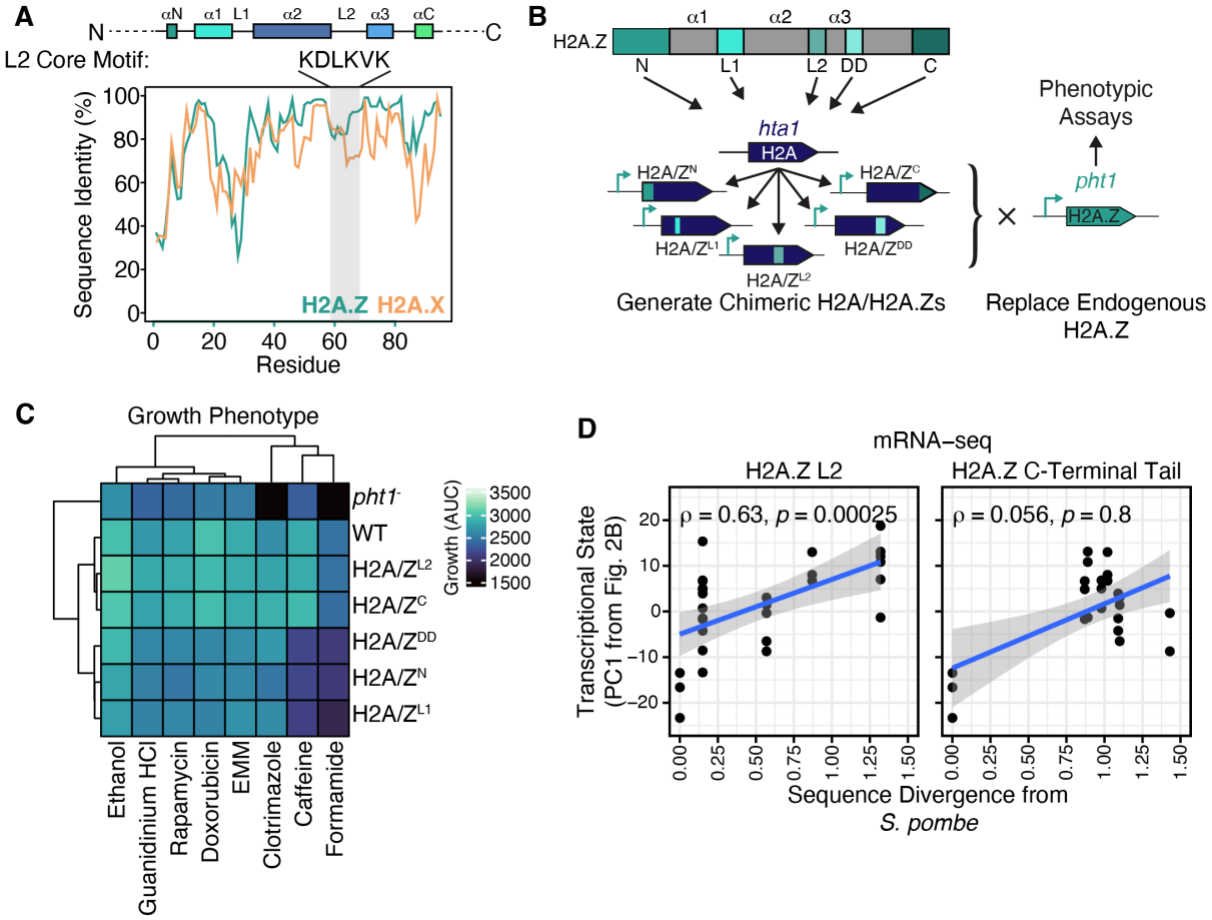
A
N
αN
α1
L1
α2
L2
α3
αC
C
L2 Core Motif:
KDLKVK
Sequence Identity (%)
100
80
60
40
20
0
H2A.Z
H2A.X
0
20
40
60
80
Residue
B
H2A.Z
α1
α2
α3
N
L1
L2
DD
C
hta1
H2A
H2A/Z^N
H2A/Z^C
H2A/Z^L1
H2A/Z^DD
H2A/Z^L2
Generate Chimeric H2A/H2A.Zs
Phenotypic Assays
pht1
H2A.Z
Replace Endogenous H2A.Z
C
Growth Phenotype
pht1-
WT
H2A/Z^L2
H2A/Z^C
H2A/Z^DD
H2A/Z^N
H2A/Z^L1
Growth (AUC)
3500
3000
2500
2000
1500
Ethanol
Guanidinium HCl
Rapamycin
Doxorubicin
EMM
Clotrimazole
Caffeine
Formamide
D
mRNA–seq
H2A.Z L2
H2A.Z C-Terminal Tail
ρ = 0.63, p = 0.00025
ρ = 0.056, p = 0.8
Transcriptional State (PC1 from Fig. 2B)
20
10
0
−10
−20
0.00
0.25
0.50
0.75
1.00
1.25
1.50
Sequence Divergence from S. pombe

437

438

Figure 3. The L2 region of H2A.Z is a key determinant of its function. A, Mean pairwise sequence identity of H2A.Z and H2A.X residues across eukaryotes, averaged using a 3-amino acid sliding window. The L2 region is highlighted in grey on the histone secondary structure, with the core domain we identify indicated. Dashed lines indicate the N- and C-terminal tails that were not included in this analysis due to variable length and resulting gappy alignment. **B**, Experimental scheme for generation of Hta1/Pht1 chimeras. **C**, Mean growth (AUC) for four biological replicates in each indicated condition, which are as in Figure 2B. **D**, Spearman's correlation analysis between the sequence divergence from *S. pombe* Pht1 of either the L2 or C-terminal tail region and principal component 1 from mRNA-seq analysis from Figure 2B. In this analysis, the *S. pombe* Pht1 sequence corresponds to a value of zero, with a larger number corresponding to a greater divergence. See also Figure S4B.

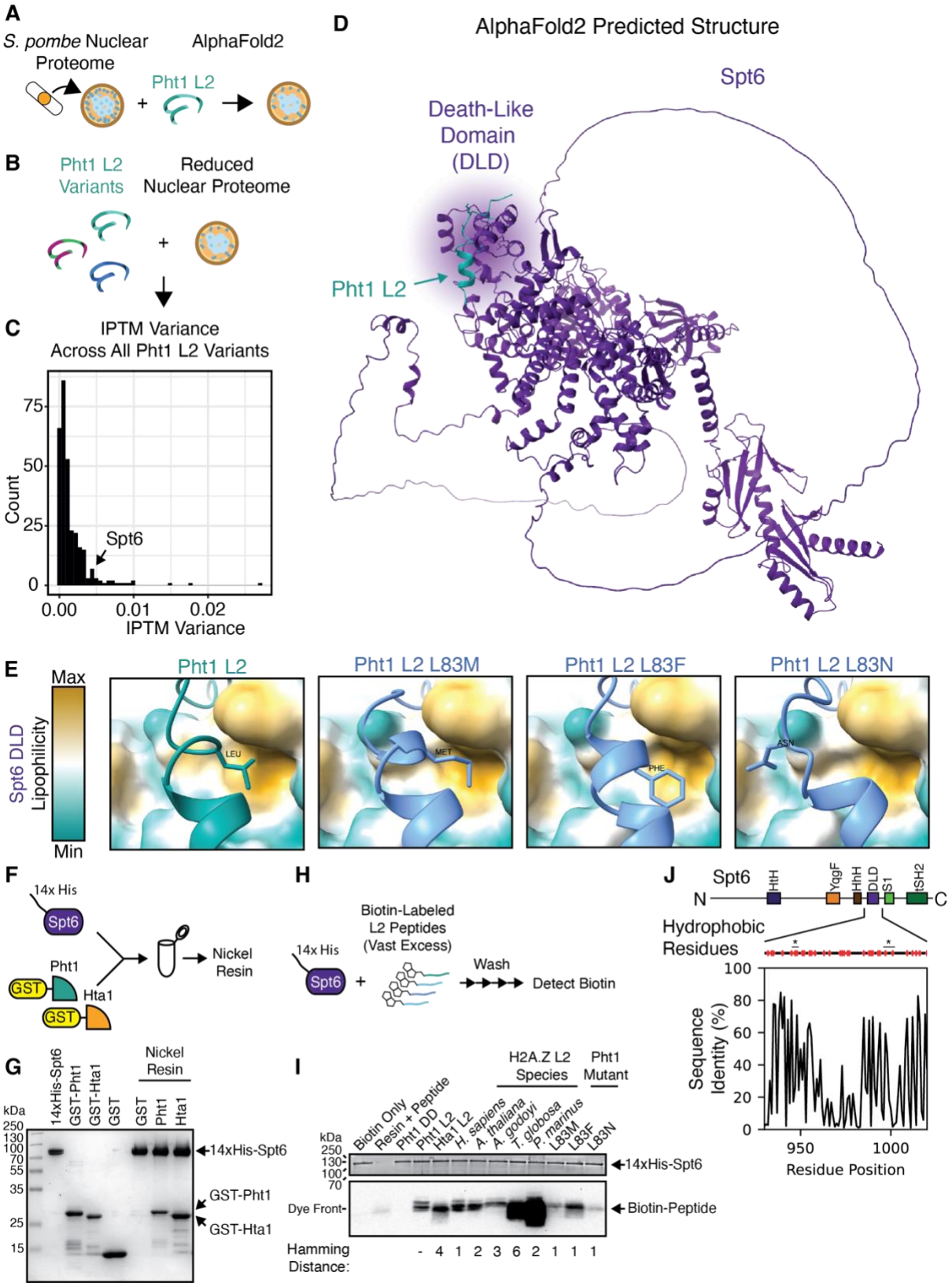
A
S. pombe Nuclear Proteome
AlphaFold2
Pht1 L2
B
Pht1 L2 Variants
Reduced Nuclear Proteome
C
IPTM Variance Across All Pht1 L2 Variants
Count
Spt6
IPTM Variance
D
AlphaFold2 Predicted Structure
Spt6
Death-Like Domain (DLD)
Pht1 L2
E
Max
Spt6 DLD Lipophilicity
Min
Pht1 L2
Pht1 L2 L83M
Pht1 L2 L83F
Pht1 L2 L83N
F
14x His
Spt6
Pht1
GST
Hta1
Nickel Resin
H
Biotin-Labeled L2 Peptides (Vast Excess)
14x His
Spt6
Wash
Detect Biotin
J
Spt6
N
C
Hydrophobic Residues
Sequence Identity (%)
Residue Position
G
Nickel Resin
14xHis-Spt6
GST-Pht1
GST-Hta1
GST
Pht1
Hta1
kDa
14xHis-Spt6
GST-Pht1
GST-Hta1
I
H2A.Z L2 Species
Pht1 Mutant
Biotin Only
Resin + Peptide
Pht1 DD
Pht1 L2
Hta1 L2
H. sapiens
A. thaliana
A. godoyi
T. globosa
P. marinus
L83M
L83F
L83N
kDa
14xHis-Spt6
Dye Front
Biotin-Peptide
Hamming Distance:
- 4 1 2 3 6 2 1 1 1

451

452

Figure 4. The L2 region of H2A.Z binds to transcription elongation factor Spt6. A, Scheme explaining the AlphaFold2 virtual interaction screen against *S. pombe* Pht1. **B,** Scheme explaining the AlphaFold2 approach used to calculate the IPTM variance for 17 Pht1 L2 variants, which is plotted in **C**. The reduced nuclear proteome was defined by the top 500 WT *S. pombe* H2A.Z interactors from (A). **D,** AlphaFold2 predicted structure of the Pht1 L2 interaction with Spt6, with the the death-like-domain (DLD) highlighted with shading. **E,** Example AlphaFold2 structures of *S. pombe* Pht1, Hta1, and Pht1 mutants. Spt6 DLD is colored with a lipophilicity surface, and each H2A position 83 (e.g. L83 for Pht1) is labelled to highlight its interaction with the Spt6 hydrophobic groove. **F,** Experimental scheme for *in vitro* interaction assays of full-length GST-Pht1, GST-Hta1, with 14xHis-Spt6(282-1159). **G,** Coomassie-stained SDS-PAGE gel of Ni-NTA-pulldowns of recombinant *S. pombe* GST-Pht1 or GST-Hta1 with *S. pombe* His-Spt6(282-1159). Detection done with colloidal Coomassie staining. **H,** Experimental scheme showing the pulldown experiment modified for biotinylated peptides. **I,** Binding assay of Pht1-derived peptides to *S. pombe* 14xHis-Spt6(282-1159) immobilized on Ni-NTA resin. Detection was done either by colloidal Coomassie staining (for 14xHis-Spt6 loading control) or by a streptavidin-HRP conjugate (for biotinylated peptides). Representative of five experiments, each with similar results. **J,** Conservation analysis of Spt6 DLD. Conservation is calculated as the mean pairwise amino acid identity across Spt6 orthologs (see Methods). The location of hydrophobic residues are highlighted in red, with those predicted to interact with Pht1 L2 further indicated by an asterisks (*). The following residues are considered as hydrophobic for the purpose of this analysis: A, V, I, L, F, M, W, Y.

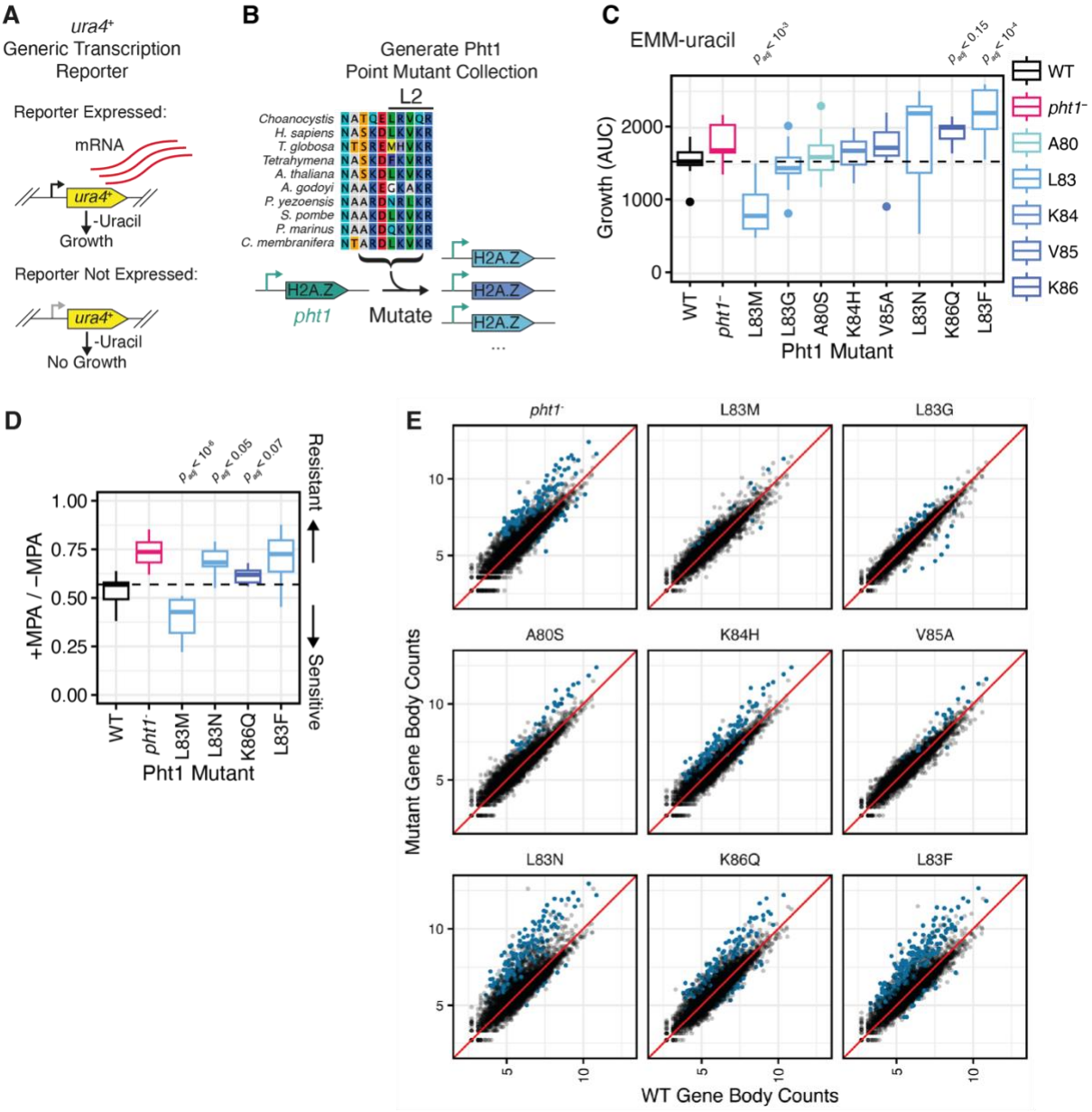
A
ura4+
Generic Transcription Reporter
Reporter Expressed:
mRNA
ura4+
-Uracil
Growth
Reporter Not Expressed:
ura4+
-Uracil
No Growth
B
Generate Pht1 Point Mutant Collection
L2
Choanocystis
H. sapiens
T. globosa
Tetrahymena
A. thaliana
A. godoyi
P. yezoensis
S. pombe
P. marinus
C. membranifera
H2A.Z
pht1
Mutate
C
EMM-uracil
Growth (AUC)
Pht1 Mutant
WT
pht1-
L83M
L83G
A80S
K84H
V85A
L83N
K86Q
L83F
A80
L83
K84
V85
K86
D
+MPA / −MPA
Resistant
Sensitive
Pht1 Mutant
E
pht1-
L83M
L83G
A80S
K84H
V85A
L83N
K86Q
L83F
Mutant Gene Body Counts
WT Gene Body Counts

475

476

Figure 5. H2A.Z L2 sequence variation explains species-specific effects on transcription. **A,** Experimental scheme explaining the *ura4*$^{+}$ reporter gene. **B,** Experimental scheme describing the generation of H2A.Z point mutants. **C,** Growth of H2A.Z point mutant strains bearing the transcriptional reporter from (D) in EMM-Uracil. The mean of WT is represented with a dashed line. Each boxplot represents 12 biological replicates, adjusted *p*-values (p_{adj}) are calculated using a two-way ANOVA followed by a post-hoc Tukey test. **D,** Growth of indicated *S. pombe* Pht1 mutants in the presence of 12.5 µM mycophenolic acid (MPA) expressed as the ratio of their paired growth in the absence of the drug. Data are 9 biological replicates and experiment was repeated three times with similar results. Boxplots represent the median bounded by quartiles. Adjusted *p*-values (p_{adj}) are calculated using a two-way ANOVA followed by a post-hoc Tukey test. **E,** Differential count analysis for gene body qPRO-seq signal calculated using DESeq2. Red line, diagonal (Y=X) line drawn to aid in interpretation. Statistically significant (p_{adj}<0.1) changes are indicated in blue.

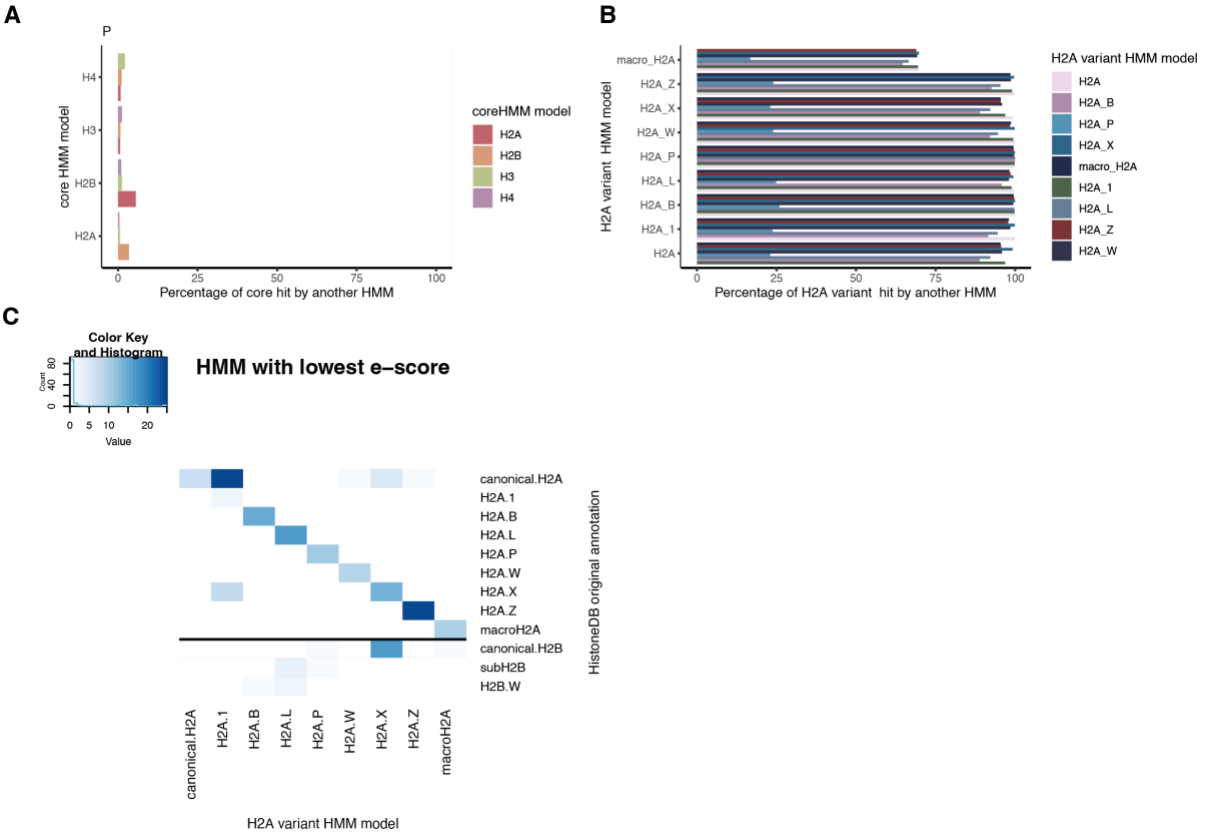
A
P
core HMM model
H4
H3
H2B
H2A
0
25
50
75
100
Percentage of core hit by another HMM
coreHMM model
H2A
H2B
H3
H4
B
H2A variant HMM model
macro_H2A
H2A_Z
H2A_X
H2A_W
H2A_P
H2A_L
H2A_B
H2A_1
H2A
Percentage of H2A variant hit by another HMM
H2A variant HMM model
H2A
H2A_B
H2A_P
H2A_X
macro_H2A
H2A_1
H2A_L
H2A_Z
H2A_W
C
Color Key and Histogram
Count
Value
HMM with lowest e−score
canonical.H2A
H2A.1
H2A.B
H2A.L
H2A.P
H2A.W
H2A.X
H2A.Z
macroH2A
canonical.H2B
subH2B
H2B.W
HistoneDB original annotation
H2A variant HMM model

Figure S1. Related to Figure 1. A, Specificity of core histone HMMs queried against histones in EukProt. **B,** Specificity of H2A variant HMM models queried against histones in EukProt. **C,** H2A variant HMMs do not reliably identify the right H2A variant, even if assigning variant identify based on the lowest E-value.

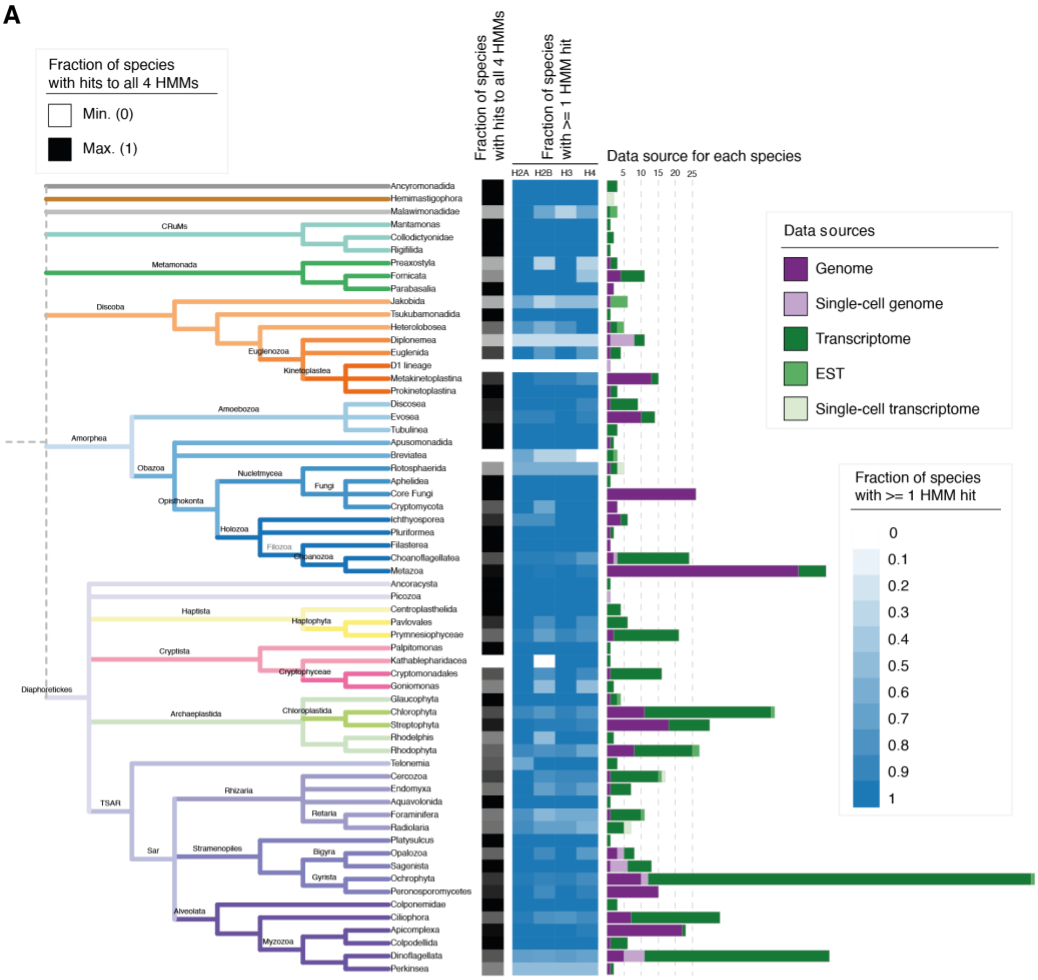
A
Fraction of species with hits to all 4 HMMs
Min. (0)
Max. (1)
Fraction of species with hits to all 4 HMMs
Fraction of species with >= 1 HMM hit
H2A H2B H3 H4
Data source for each species
5 10 15 20 25
Data sources
Genome
Single-cell genome
Transcriptome
EST
Single-cell transcriptome
Fraction of species with >= 1 HMM hit
0
0.1
0.2
0.3
0.4
0.5
0.6
0.7
0.8
0.9
1
Ancyromonadida
Hemimastigophora
Malawimonadidae
CRuMs
Mantamonas
Collodictyonidae
Rigifilida
Metamonada
Preaxostyla
Fornicata
Parabasalia
Discoba
Jakobida
Tsukubamonadida
Heterolobosea
Euglenozoa
Diplonemea
Euglenida
Kinetoplastea
D1 lineage
Metakinetoplastina
Prokinetoplastina
Amoebozoa
Discosea
Evosea
Tubulinea
Amorphea
Apusomonadida
Breviatea
Obazoa
Rotosphaerida
Nucletmycea
Aphelidea
Fungi
Core Fungi
Opisthokonta
Cryptomycota
Ichthyosporea
Holozoa
Pluriformea
Filasterea
Filozoa
Choanozoa
Choanoflagellatea
Metazoa
Ancoracysta
Picozoa
Haptista
Centroplasthelida
Haptophyta
Pavlovales
Prymnesiophyceae
Palpitomonas
Cryptista
Kathablepharidacea
Cryptophyceae
Cryptomonadales
Goniomonas
Diaphoretickes
Glaucophyta
Archaeplastida
Chloroplastida
Chlorophyta
Streptophyta
Rhodelphis
Rhodophyta
Telonemia
Cercozoa
TSAR
Rhizaria
Endomyxa
Aquavolonida
Retaria
Foraminifera
Radiolaria
Sar
Stramenopiles
Platysulcus
Bigyra
Opalozoa
Sagenista
Gyrista
Ochrophyta
Peronosporomycetes
Alveolata
Colponemidae
Ciliophora
Myzozoa
Apicomplexa
Colpodellida
Dinoflagellata
Perkinsea

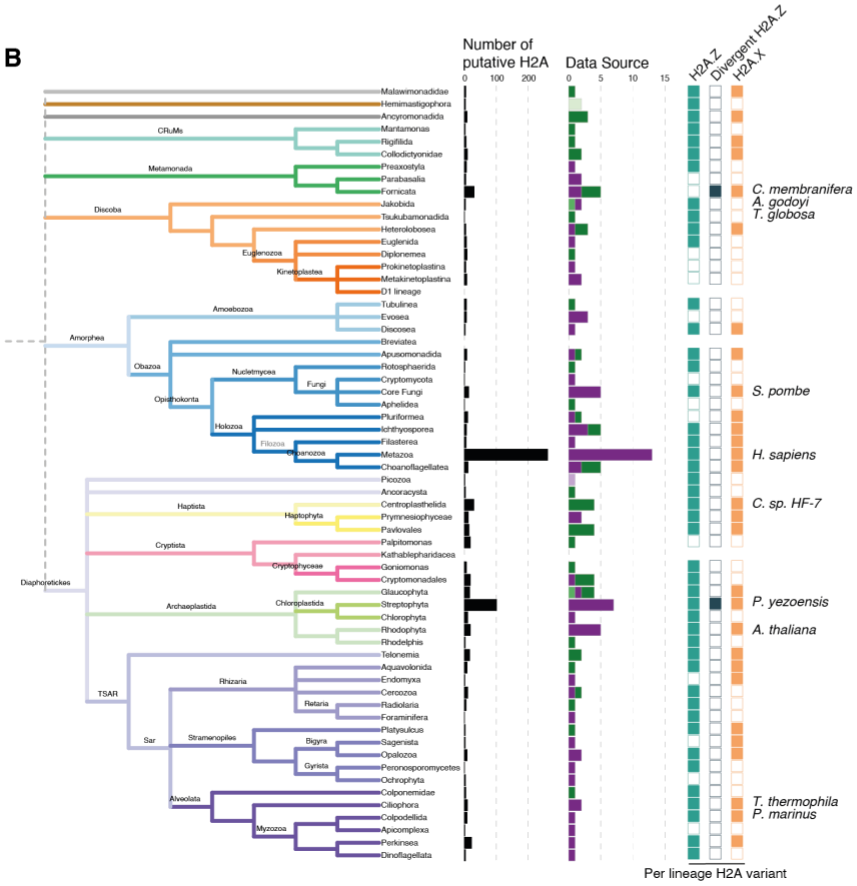
B
Number of putative H2A
0 100 200
Data Source
0 5 10 15
H2A.Z
Divergent H2A.Z
H2A.X
Malawimonadidae
Hemimastigophora
Ancyromonadida
CRuMs
Mantamonas
Rigifilida
Collodictyonidae
Metamonada
Preaxostyla
Parabasalia
Fornicata
Discoba
Jakobida
Tsukubamonadida
Heterolobosea
Euglenozoa
Euglenida
Diplonemea
Kinetoplastea
Prokinetoplastina
Metakinetoplastina
D1 lineage
Amoebozoa
Tubulinea
Evosea
Discosea
Amorphea
Breviatea
Apusomonadida
Obazoa
Rotosphaerida
Nucletmycea
Cryptomycota
Fungi
Core Fungi
Opisthokonta
Aphelidea
Holozoa
Pluriformea
Ichthyosporea
Filozoa
Filasterea
Choanozoa
Metazoa
Choanoflagellatea
Picozoa
Ancoracysta
Haptista
Centroplasthelida
Haptophyta
Prymnesiophyceae
Pavlovales
Cryptista
Palpitomonas
Kathablepharidacea
Cryptophyceae
Goniomonas
Cryptomonadales
Diaphoretickes
Glaucophyta
Archaeplastida
Chloroplastida
Streptophyta
Chlorophyta
Rhodophyta
Rhodelphis
Telonemia
Aquavolonida
Rhizaria
Endomyxa
Cercozoa
TSAR
Retaria
Radiolaria
Foraminifera
Platysulcus
Sar
Stramenopiles
Bigyra
Sagenista
Opalozoa
Gyrista
Peronosporomycetes
Ochrophyta
Colponemidae
Alveolata
Ciliophora
Colpodellida
Myzozoa
Apicomplexa
Perkinsea
Dinoflagellata
C. membranifera
A. godoyi
T. globosa
S. pombe
H. sapiens
C. sp. HF-7
P. yezoensis
A. thaliana
T. thermophila
P. marinus
Per lineage H2A variant

499

Figure S2. Related to Figure 1. A, Overview of histones identified by different core histone HMMs in the context of eukaryotic phylogeny. **B,** Number of H2As and presence/absence of specific variants (H2A.Z, H2A.X, divergent H2A.Z, as mentioned in the main text) across eukaryotic phylogeny. Numbers reflect the distribution in the final filtered dataset. The cladogram of major eukaryotic lineages and information on data sources are taken from EukProt. H2A.Z from the list of species in the far right column were chosen for further investigation.

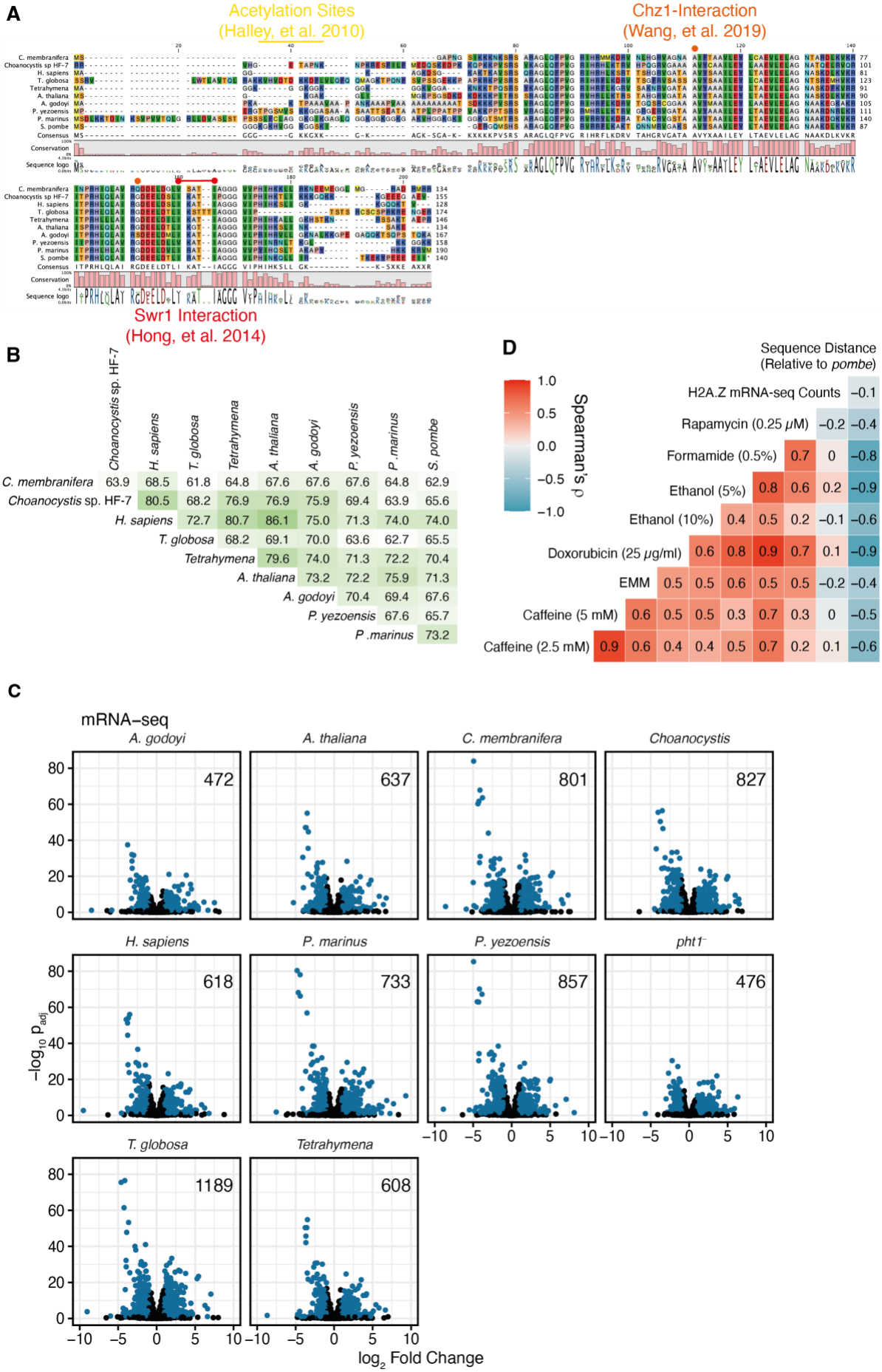
A
Acetylation Sites
(Halley, et al. 2010)
Chz1-Interaction
(Wang, et al. 2019)
Swr1 Interaction
(Hong, et al. 2014)
B
Choanocystis sp. HF-7
H. sapiens
T. globosa
Tetrahymena
A. thaliana
A. godoyi
P. yezoensis
P. marinus
S. pombe
C. membranifera 63.9 68.5 61.8 64.8 67.6 67.6 67.6 64.8 62.9
Choanocystis sp. HF-7 80.5 68.2 76.9 76.9 75.9 69.4 63.9 65.6
H. sapiens 72.7 80.7 86.1 75.0 71.3 74.0 74.0
T. globosa 68.2 69.1 70.0 63.6 62.7 65.5
Tetrahymena 79.6 74.0 71.3 72.2 70.4
A. thaliana 73.2 72.2 75.9 71.3
A. godoyi 70.4 69.4 67.6
P. yezoensis 67.6 65.7
P .marinus 73.2
D
Spearman's ρ
1.0
0.5
0.0
−0.5
−1.0
Sequence Distance
(Relative to pombe)
H2A.Z mRNA-seq Counts −0.1
Rapamycin (0.25 μM) −0.2 −0.4
Formamide (0.5%) 0.7 0 −0.8
Ethanol (5%) 0.8 0.6 0.2 −0.9
Ethanol (10%) 0.4 0.5 0.2 −0.1 −0.6
Doxorubicin (25 μg/ml) 0.6 0.8 0.9 0.7 0.1 −0.9
EMM 0.5 0.5 0.6 0.5 0.5 −0.2 −0.4
Caffeine (5 mM) 0.6 0.5 0.5 0.3 0.7 0.3 0 −0.5
Caffeine (2.5 mM) 0.9 0.6 0.4 0.4 0.5 0.7 0.2 0.1 −0.6
C
mRNA−seq
A. godoyi 472
A. thaliana 637
C. membranifera 801
Choanocystis 827
H. sapiens 618
P. marinus 733
P. yezoensis 857
pht1⁻ 476
T. globosa 1189
Tetrahymena 608
−log10 padj
log2 Fold Change

508

Figure S3. Related to Figure 2. A, Alignment of representative H2A.Z sequences taken from our phylogeny, with key residues and relevant literature noted. **B,** Pairwise percent identity of representative H2A.Zs, excluding N- and C-terminal tail regions. **C,** Differential expression analysis of mRNA-seq data for each species's H2A.Z replacement line against WT *S. pombe*. Number of differentially expressed genes (p_{adj}<0.1, out of 5134 coding genes) is indicated for each panel. **D,** Spearman's correlations for the phenotypes of H2A.Z replacement lines from (2B) with themselves, as well as either their sequence distance from WT *S. pombe* or their expression.

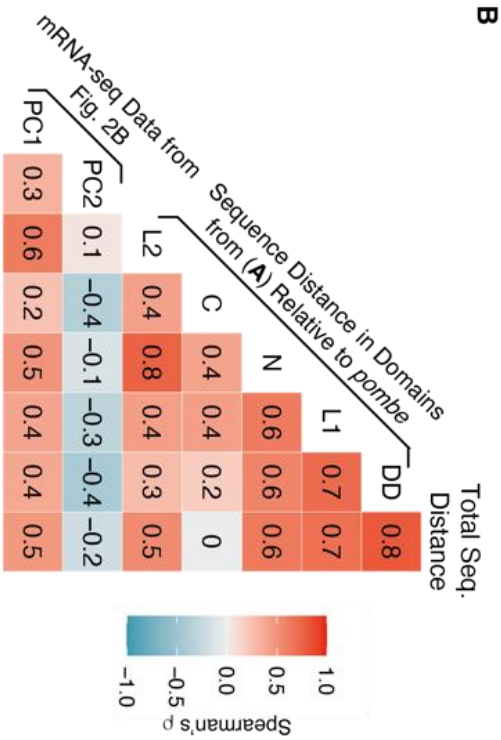
A
αN
α1
L1
α2
L2
α3
αC
H2A Coordinates
H2A.Z Coordinates
N
L1
L2
DD
C
hta1 (+1)
htaZ (+1)
pht1 (+1)
Consensus
Conservation
Sequence logo
B
Total Seq. Distance
Sequence Distance in Domains from (A) Relative to pombe
mRNA-seq Data from Fig. 2B
DD 0.8
L1 0.7 0.7
N 0.6 0.6 0.6
C 0.4 0.4 0.2 0
L2 0.4 0.8 0.4 0.3 0.5
PC2 0.1 −0.4 −0.1 −0.3 −0.4 −0.2
PC1 0.3 0.6 0.2 0.5 0.4 0.4 0.5
Spearman's ρ
1.0
0.5
0.0
−0.5
−1.0

Figure S4. Related to Figure 4. A, Alignment of *S. pombe* H2A and H2A.Z identifying the five regions used to generate chimeras from (3A). **B,** Additional Spearman's correlation analyses of mRNA-seq data from (2B) against the sequence distance for each complemented H2A.Z in the indicated regions from (A).

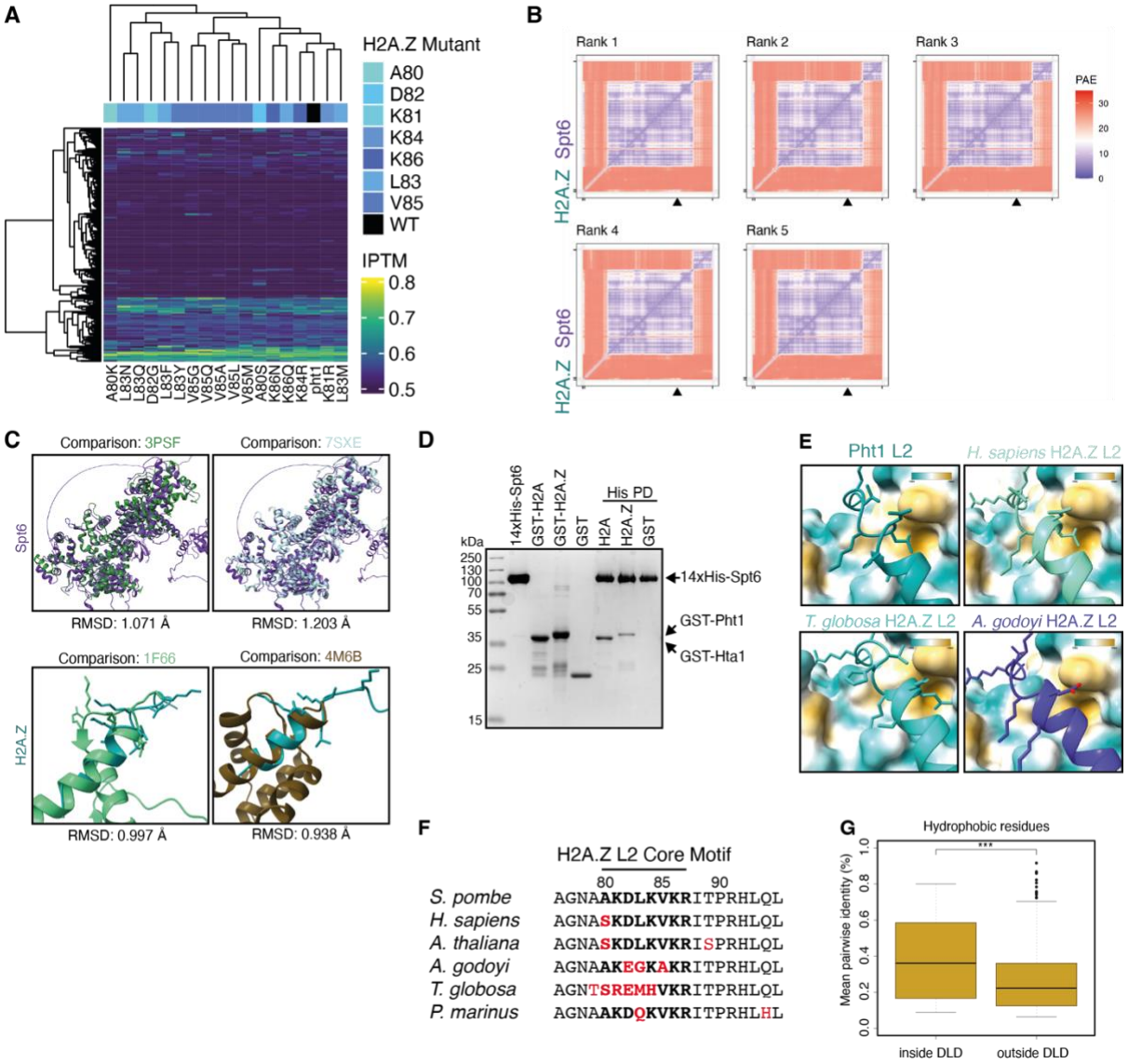
A
H2A.Z Mutant
A80
D82
K81
K84
K86
L83
V85
WT
IPTM
0.8
0.7
0.6
0.5
A80K
L83N
L83Q
D82G
L83F
L83Y
V85G
V85Q
V85A
V85L
V85M
A80S
K86N
K86Q
K84R
pht1
K81R
L83M
B
Rank 1
Rank 2
Rank 3
Rank 4
Rank 5
PAE
30
20
10
0
H2A.Z Spt6
H2A.Z Spt6
C
Comparison: 3PSF
Comparison: 7SXE
Spt6
RMSD: 1.071 Å
RMSD: 1.203 Å
Comparison: 1F66
Comparison: 4M6B
H2A.Z
RMSD: 0.997 Å
RMSD: 0.938 Å
D
14xHis-Spt6
GST-H2A
GST-H2A.Z
GST
His PD
H2A
H2A.Z
GST
kDa
250
130
100
70
55
35
25
15
14xHis-Spt6
GST-Pht1
GST-Hta1
E
Pht1 L2
H. sapiens H2A.Z L2
T. globosa H2A.Z L2
A. godoyi H2A.Z L2
F
H2A.Z L2 Core Motif
80 85 90
S. pombe AGNAAKDLKVKRITPRHLQL
H. sapiens AGNASKDLKVKRITPRHLQL
A. thaliana AGNASKDLKVKRISPRHLQL
A. godoyi AGNAAKEGKAKRITPRHLQL
T. globosa AGNTSREMHVKRITPRHLQL
P. marinus AGNAAKDQKVKRITPRHLHL
G
Hydrophobic residues
***
Mean pairwise identity (%)
0.0
0.2
0.4
0.6
0.8
1.0
inside DLD
outside DLD

524

Figure S5. Related to Figure 4. A, AlphaFold2 predicted interaction scores (IPTM) for the top-500 predicted H2A.Z-interacting proteins in *S. pombe* across all tested H2A.Z L2 mutants, as well as H2A and WT H2A.Z. **B,** AlphaFold2 predicted error alignment (PAE) for the 5 replicate models of WT *S. pombe* Pht1 against *S. pombe* Spt6. **C,** Comparison of AlphaFold2 predicted *S. pombe* Spt6 structure to either the crystal structure of *S. cerevisiae* (PDB 3PSF) or Cryo-EM structure of *Pichia pastoris* Spt6 (7XSE), as well as predicted Pht1 L2 against the structure of either *H. sapiens* H2A.Z.1 (PDB 1F66) or *S. cerevisiae* Htz1 (PDB 4M6B. **D,** As in Figure 4G, but with 300 mM NaCl. **E,** Example AlphaFold structures for *S. pombe* Pht1 and H2A.Z L2s from selected species, with Spt6 being represented as a lipophilicity surface as in (Fig. 4D). **F,** Alignment of peptides used in experiments for Figure 4I, with the L2 core motif highlighted with bold text, and amino acid differences from S. pombe Pht1 indicated in red. Numbering corresponds to the position of the given amino acid in Pht1. **G,** Hydrophobic residue conservation analysis. Mean pairwise sequence identity for hydrophobic residues within vs. outside of the Spt6 DLD. The following residues are considered as hydrophobic for the purpose of this analysis: A, V, I, L, F, M, W, Y. Statistical significance (*** $p<0.005$) was calculated with a Wilcoxon test.

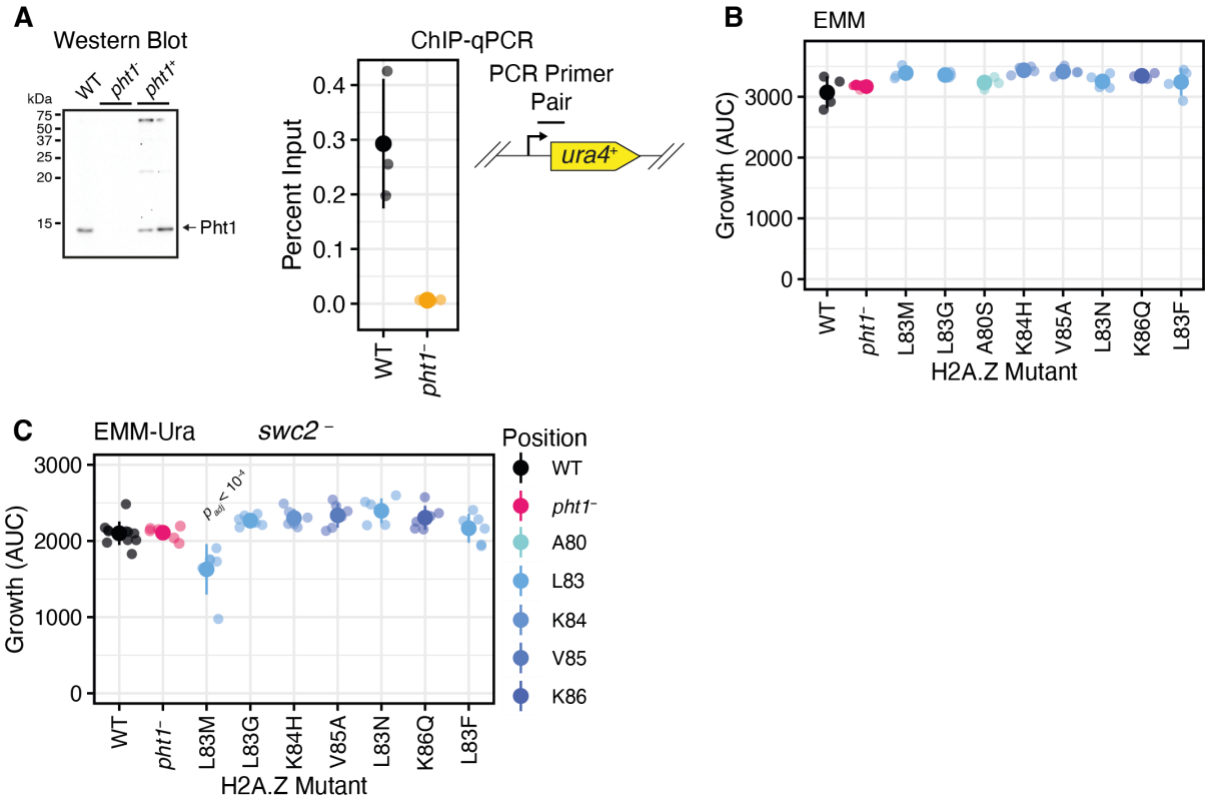
A
Western Blot
WT
pht1-
pht1+
kDa
75
50
37
25
20
15
Pht1
ChIP-qPCR
Percent Input
0.4
0.3
0.2
0.1
0.0
WT
pht1-
PCR Primer Pair
ura4+
B
EMM
Growth (AUC)
3000
2000
1000
0
WT
pht1-
L83M
L83G
A80S
K84H
V85A
L83N
K86Q
L83F
H2A.Z Mutant
C
EMM-Ura
swc2 -
Growth (AUC)
3000
2000
1000
0
WT
pht1-
L83M
L83G
K84H
V85A
L83N
K86Q
L83F
H2A.Z Mutant
Position
WT
pht1-
A80
L83
K84
V85
K86

542

543

Figure S6. Related to Figure 5. A, ChIP-qPCR data for *ura4*$^{+}$ reporter in either WT or *pht1*$^{-}$ cells. Plotted are data from three independent ChIP experiments and are the average of 4 technical replicates. **B,** Growth of H2A.Z point mutant strains in the absence of selection (EMM). Plotted are four biological replicates, with their mean and standard error. **C,** As in Figure 5C, but in a *swc2*$^{-}$ background. Plotted are 5 biological replicates with their mean and standard error. P_{adj} is calculated as a Tukey post-hoc test of a 2-way ANOVA.

SUPPLEMENTARY TABLES AND DATA FILES LEGENDS

Supplementary Data Table S1. Pan-H2A dataset annotations, related to Supplementary Data File S1.

Supplementary Data Table S2. AlphaFold2 multimer IPTM vs. PTM predictions for *S. pombe* Pht1 L2 mutants against *S. pombe* nuclear proteins.

Supplementary Data Table S3. AlphaFold2 multimer IPTM vs. PTM predictions for H2A.Z L2 mutants against *S. pombe* nuclear proteins.

Supplementary Data Table S4. *Schizosaccharomyces pombe* strains used in this study.

Supplementary Data File S1. Pan-H2A sequence database used in this study.

Supplementary Data File S2. Representative H2A.Z sequences used in this study.

Supplementary Data File S3. Spt6 sequence database used in this study.

METHODS

Histone Dataset construction

To investigate H2A.Z sequence diversity across eukaryotes, we sought to identify H2A.Z orthologs using a phylogenetic approach. First, to identify proteins homologous to a specific core histone (i.e. to H2A rather than H2B, H3, or H4), we used HHMer[93] to build specific HMM models (command = hmmbuild --amino) for each of the four core histones from curated histone sequences in HistoneDB 2.0.[94] The resulting models retrieve all except one histone variant in HistoneDB (H2A.P from *Heterocephalus glaber*, annotated as 'Huntingtin-interacting protein M') and hit the wrong core histone in only three instances. This suggests that the models are both sensitive and specific and can be used to discriminate different core histones from each other with reasonably accuracy. We therefore proceeded to search for hits against each model (hmmsearch –noali) in the EukProt protein database (v2, accessed on 01-12-2020),[95] retaining only hits with an E-value < 0.001. With this filter, the probability that a given histone is hit by more than one core histone-specific HMM is relatively low (Fig. S1A).

To determine whether separate HMM models for each H2A *variant* could be used to identify H2A *variants* by homologous search alone, we build models in the same manner as above (using curated H2A variants from HistoneDB) and then searched EukProt and HistoneDB 2.0. Variant HMM models hit the correct HistoneDB H2A variant in most instances, but a given variant is often also hit by additional variant models (Fig. S1B). Even though E-values can be used to identify the correct variant in most instances (Fig. S1C), we consider this level of specificity insufficient for robust identification of H2A variants and therefore proceeded with homologs identified by the initial H2A HMM as the starting point for tree building. Histones also hit by another core histone HMM were only retained if the H2A model returned the best E-value.

Tree building

To facilitate tree building, we only retained putative H2A orthologs shorter than 400 amino acids and only considered H2As from species with hits against all four core histone HMMs (568 out of 742 species). Some species, including metazoa and plants, encode many more H2A paralogs than others. To balance the dataset, we retained a maximum of five species per supergroup, eliminating species semi-randomly (prioritising coverage of different Eukprot lineages). The resulting dataset contains 839 putative H2As from 127 species (Fig. 1).

These putative H2A sequences were aligned using MAFFT (command= mafft --localpair --maxiterate 1000).[96] ModelTest-NG[97] was used to determine the best fit model of evolution to be used for tree building (WAG+G4), which was done using RAxML-NG (command = raxml-ng --msa --model WAG+G4 --seed 2)[98]. Sequences associated with long branches (Fig. 1A) were manually inspected but not removed as their presence does not affect conclusions. Trees were plotted using iTOL.[99]

Sequence conservation of Spt6

S. pombe Spt6 (Uniprot ID: Q09915) is part of EukProt orthogroup OG0001365. Sequences belonging to this orthogroup were downloaded (12-2-2024) and filtered to only contain proteins from species also present in the final filtered H2A dataset, and further filtered to only contain one ortholog per species, retaining the proteins with the highest pairwise identity to Q09915. These sequences were aligned using MAFFT-linsi and conservation assayed as average pairwise sequence identity at residues present in Q09915.

Yeast Culture, Strain Manipulation, and Phenotypic Assays

All strains used in this study are listed in Supplementary Table S4. Yeast (*S. pombe* 972 *h*-) were cultured under standard conditions (32 ºC). Unless otherwise stated, media used were

either EMM2 (Edinburgh Minimal Media)[100] or YES (Yeast Extract with Supplements)[101] for *S. pombe*.

S. pombe strains were manipulated either using one-step PCR-based HR mutagenesis[102] or the SpEDIT CRISPR editing platform.[103] For both, heat-shock was used to transform chemically-competent parent strains.[104] Donor templates for homologous recombination were prepared using either Gibson assembly[105] using reagents supplied by the IMP Molecular Biology Service combined, with site directed mutagenesis, or by direct synthesis from commercial vendors (IDT, Genscript). All manipulations were verified by PCR genotyping and where appropriate sequencing of the relevant locus.

Phenotypic assays in this study were performed using a plate-based bulk growth assay. OD_{600} was monitored in 384-well plates (Nunc) continuously under the stress conditions indicated in figure legends at the standard growth temperature with shaking. Saturated cultures were sub-cultured 100-fold, and all assays were performed in either EMM complete, EMM without uracil (EMM-Ura), or YES. Data collection was performed on a BioTek Epoch2. Area under the curve (AUC) was calculated from these growth curves in R using the Growthcurver package (https://cran.r-project.org/web/packages/growthcurver/vignettes/Growthcurver-vignette.html). All subsequent data analysis was done in R.

Antibody Generation, Protein Purification, and Analysis

A polyclonal antibody was raised in rabbit against *S. pombe* H2A.Z (Pht1) using a C-terminal-tail targeting peptide chosen based on predicted immunogenicity, and that it avoided the sequence domains of interest in the present study. Briefly, polyclonal serum was commercially produced (Eurogentec) using the peptide N-CLIRTKEKYPEEEEII-C. Antibodies were affinity purified using the same peptide. Briefly, SulfoLink agarose gel (Pierce Cat. No. 20401) was equilibrated in coupling buffer (50 mM Tris pH 8.5, 5 mM EDTA) before

645 indubating with peptide for 90 min at RT. Afterwards, b-Marcapthoethanol was added and
646 beads were incubated for 15 min at RT. Coupled beads were then washed three times in
647 coupling buffer before adding serum diluted with 2 volumes of PBS with 0.2% tween-20.
648 Beads and serum were then incubated together for three hours at RT with rotation. Beads were
649 then collected in a disposable column and washed 6 times with PBS with 0.2% tween-20. To
650 elute antibody, 750 µl of 0.1 M Glycine was added, incubated for 1 min, then allowed to flow
651 through. Eluates were immediately quenched with 250 µl of 1 M K_2HPO_4. Elution was repeated
652 nine additional times for a total of 10 fractions. Antibody-containing fractions were detected
653 using Nanodrop spectrophotometer, pooling the highest concentration eluates. Antibodies were
654 verified using *S. pombe* H2A.Z knockout strains (*pht1*$^-$) for both Western blot and ChIP
655 applications (Fig. S6A), and aliquoted antibodies were stored at -80 ºC.

656 All recombinant proteins were produced by the Vienna BioCenter Core Facilities
657 Protein Technologies Facility using constructs commercially synthesized (Genscript) in
658 *Escherichia coli* BL21(DE3). *S. pombe* Hta1 and Pht1 were produced as full-length N-terminal
659 GST fusions (PZH_668 and PZH_669). For *S. pombe* Spt6 a truncated version corresponding
660 to residues 282–1159 (PZH_670) was produced as a 14xHis tagged fusion.

661 Expression was performed by autoinduction in TB media with 1.5% lactose and 50
662 µg/ml kanamycin for 24 hrs at 25 ºC with shaking. Cells were lysed by sonication (Sonics
663 VCX-750, 24-element probe: 3 mm, amplitude: 50%, time: 1 min, pulse-on: 1 s, pulse-off: 2
664 s) in the following buffer: 50 mM Tris-HCl pH 8.0, 500 mM NaCl, 5 mM DTT, Benzonase (2
665 µl per ml of Lysis buffer), 2 mM MgCl2, 0.2% (v/v) NP-40 and cOmplete protease inhibitor
666 tablets (Roche, 1 tablet per 25 ml of lysis buffer).

667 *S. pombe* Pht1 and Hta1 were purified by glutathione affinity chromatography. Each
668 supernatant was mixed with 100 µl of Glutathione Sepharose 4 FF (Cytiva Cat. No. 17513203,
669 previously equilibrated with binding buffer A (50 mM Tris-HCl pH 8.0, 500 mM NaCl and 5

mM DTT)) for 2h at 4 °C in a tube rotator. The beads were washed with 3 ml of binding buffer A. The protein was eluted with 400 µl of elution buffer A (50 mM Tris-HCl pH 8.0, 500 mM NaCl, 5 mM DTT and 10 mM reduced Glutathione). For GST-Hta1, the GST-elution was dialyzed against SP S buffer (25 mM HEPES pH 7.4, 100 mM NaCl, 1 mM DTT, 5% glycerol) for 18h in the cold room with constant mixing to adjust the conductivity for loading it onto 1mL HiTrap SP FF (Cytiva Cat. No. 17515701) column, pre-equilibrated with SP S buffer**,** at a flow rate of 1 ml/min. The column was then washed with SP S buffer until UV returned to baseline and the protein was eluted in a gradient to 50% of SP E buffer (25 mM HEPES pH 7.4, 1 M NaCl, 1 mM DTT, 5% glycerol) over 50 mL. Eluates were pooled and concentrated to a final volume of 1.5 mL using Vivaspin 20 MWCO 30 kDa (Sartorius Cat. No. VS2021). Concentrated pool eluates were then loaded onto a Superdex 200 16/60 (Cytiva Cat. No. 28989335) at a flow rate of 1 ml per minute previously equilibrated with SEC buffer (50 mM Tris pH 8.0, 150 mM NaCl, 1 mM DTT, 5% glycerol), where full-length protein eluted in the void volume.

For *S. pombe* Spt6, purification was performed using immobilized metal affinity chromatography. Each supernatant was mixed with 500 µl of *Ni Sepharose 6 FF* (Cytiva Cat. No. 17531806, previously equilibrated with binding buffer B (50 mM Tris-HCl pH 8.0, 500 mM NaCl, 1 mM DTT and 20 mM imidazole)) for 2h at 4 °C in a tube rotator. The beads were washed with 1.5 ml of binding buffer B and with 1.5 ml of wash buffer B (50 mM Tris-HCl pH 8.0, 500 mM NaCl, 1 mM DTT, 80 mM imidazole). The protein was eluted with 400 µl of elution buffer B (50 mM Tris-HCl pH 8.0, 500 mM NaCl, 1 mM DTT, 500 mM imidazole). All samples were dialysed against 1 l of dialysis buffer (25 mM Tris-HCl pH 8.0, 150 mM NaCl and 1 mM DTT) at 4 °C overnight. The dialysed samples were centrifuged at 4 °C and 21000xg for 5 min.

SDS-PAGE separation was performed using self-cast gels using standard methods. Gels were stained using colloidal blue reagents (MBS Blue) provided by the Molecular Biology Service. For Western blots, proteins were transferred using a standard wet protocol to a 0.2 µm nitrocellulose membrane (Cytiva Cat. No. 10600004), blocking in 5% non-fat dry milk (Maresi) dissolved in TBS^T. Anti-Pht1 antibody was used at 1:1000 diluted in blocking buffer and detected using chemiluminesce following incubation with anti-rabbit HRP conjugates (Biorad Cat. No. 1706515), which were diluted 1:10,000 in blocking buffer. Imaging of gels and Western blots was performed using a Thermo Fisher iBright 1500 imaging system.

In vitro pulldown experiments

Recombinantly expressed and purified proteins were bound to 10 µl Ni-NTA (Qiagen Cat. No. 30210) resin previously equilibrated in pulldown buffer (50 mM Tris pH 8, 150 mM NaCl, 2.5 mM DTT, 0.1% tween-20). Bait proteins were then bound to the prepared resins for 1 hr at RT. For *S. pombe* Hta1 and Pht1 experiments, 10 µg was used. For *S. pombe* Spt6, 25-50 µg was used. For peptide experiments, a vast excess (50 µg) of biotinylated peptide was used. The resins were then washed 4 times with pulldown buffer, then the prey protein was added, incubating for 2 hrs at RT. Beads were then washed 4 times, then proteins were eluted from the beads by boiling in SDS-PAGE running buffer. Proteins were then separated on an SDS-PAGE gel and analyzed by either colloidal blue staining or Western blot as indicated above, using a streptavidin-HRP conjugate (Invitrogen Ca. No. S911) for detection.

mRNA Sequencing Library Preparation and Analysis

Total RNA was extracted from yeast strains grown to mid-exponential phase (OD_{600} ~0.5) using a standard hot acid phenol protocol. Libraries were then prepared by polyA-tail enrichment using the NEBNext Ultra II Directional RNA Library Prep Kit for Illumina (NEB

Cat. No. E7760L) with the polyA selection module (NEB Cat. No. E7490L). Size selection steps and final library cleanup were performed using the NA clean-up bead solution provided by the VBC core facilities, which is adapted from DeAngelis et al. 1995[106] using carboxylate-modified Sera-Mag Speed beads (Cytiva). Library quality control was performed using the Advanced Analytical Fragment Analyzer using the HS NGS fragment analysis kit (Agilent Cat. No. DNF-474) as well as qPCR using reagents produced by the Molecular Biology Service in conjunction with commercial DNA standards (Roche Cat. No KK4903). Data were collected on a Thermo Scientific QuantStudio5 instrument.

Prepared libraries were sequenced on either an Illumina NextSeq2000 or NovaSeq S4 at the Vienna BioCenter Core Facilities Next Generation Sequencing Core using paired-end mode. Quality control of the data was performed using FastQC (Babraham Institute). Transcript-level quantification against the *S. pombe* ASM294v2 reference genome available from ENSEMBLv55 was performed using Kallisto[107]. Differential expression analysis was performed using DESeq2[108] in R, in which all subsequent data manipulation was performed.

PRO-seq Library Generation and Analysis

We performed a variant of PRO-seq, qPRO-seq, as recently published[82], with modifications[81] to make it compatible with *S. pombe*. *S. pombe* cells were grown in 10 ml YES media to OD_{600} ~0.4–0.5. Cells were then harvested by centrifugation at 400 x *g* for 5 min at 4 ºC. Cells were then resuspended in 10 ml of ice-cold PBS, spun down once more, then resuspended in 10 ml ice-cold yeast permeabilization buffer (0.5% Sarkosyl, 0.5 mM DTT, Roche cOmplete protease inhibitor cocktail, 4U/ml Invitrogen RiboLock RNAse Inhibitor). After 20 min incubation on ice, cells were once again collected by gentle centrifugation, then resuspended in 50 µl storage buffer (10 mM Tris-HCl, pH 8.0, 25% (v/v) glycerol, 5 mM $MgCl_2$, 0.1 mM EDTA, 5 mM DTT).

A 2X run-on reaction master mix (40 mM Tris pH 7.7, 64 mM MgCl2, 1 mM DTT, 400 mM KCl, 40 µM Biotin-11-CTP, 40 µM Biotin-11-UTP, 40 µM ATP, 40 µM GTP, 1% sarkosyl) was prepared and preheated to 30 ºC. To each aliquot of permeabilized cells, 50 µl of master mix and 1 µl of RNAse inhibitor were added, then mixed by gently pipetting with wide-bore pipet tips before immediately incubating at 30 ºC for 5 min. To ensure precise timing, samples were done in batches staggered by 30–60 sec. Using the Norgen RNA Extraction Kit (Cat. No. 37500), 350 µL of RL buffer were added to each sample and then vortexed. 240 µl of absolute ethanol were added, then the entire well-mixed solution was applied to the RNA extraction column. The column was spun at 3500 x *g* for 1 min at 25 ºC, then washed once with 400 µl of wash solution A. This step was repeated a second time, then the column was dried by spinning at high speed for 2 min. RNA was eluted twice in 50 µl of DEPC-treated MonoQ water, the two fractions were pooled and then briefly denatured at 65 ºC for 30 sec. After snap cooling on ice, 25 µl of ice cold 1 M NaOH were added to each sample, which was then incubated for 10 min on ice. Finally, samples were quenched with 125 µl of cold 1 M Tris-HCl pH 6.8, then cleaned up using a standard ethanol precipitation overnight. Samples were resuspended in a small volume of DEPC water (6 µl).

Meanwhile, 10 µl per sample of Dynabeads MyOne Streptavidin C1 beads (Thermo Fisher Cat. No. 65001) were prepared by washing once with bead preparation buffer (0.1 M NaOH, 50 mM NaCl), then once in bead binding buffer (10 mM Tris-HCl, pH 7.4, 300 mM NaCl, 0.1% (v/v) Triton X-100, 1 mM EDTA, RNAse inhibitors), then resuspended in 25 µl bead binding buffer.

3’RNA adapter ligation was performed by adding 1 µl 10 µM oligo VRA3 to the resuspended RNA, boiling at 65 ºC for 30 sec, then snap cooling on ice. Ligation reactions were then prepared with T4 RNA Ligase using the provided instructions. After incubating reactions at 25 ºC for 1 hr, ligated RNA was bound to the 25 µl previously prepared streptavidin

beads by adding 55 µl bead binding buffer and the entire ligation reaction. Samples were incubated for 20 min at 25 ºC, then washed once with 500 µl high salt wash buffer (50 mM Tris-HCl, pH 7.4, 2 M NaCl, 0.5% (v/v) Triton X-100, 1 mM EDTA, 2 µl/10 ml Ribolock RNAse inhibitor), transferring beads to a clean tube. Beads were then washed once more in the new tube with low salt wash buffer (5 mM Tris-HCl, pH 7.4, 0.1% (v/v) Triton X-100, 1 mM EDTA, 2 µl/10 ml Ribolock RNAse inhibitor), then resuspended in 20 µl T4 PNK reaction mix (1X T4 PNK Buffer, 1 mM ATP, 1 µl T4 PNK, 1 µl RiboLock RNAse inhibitor). Samples were then incubate at 37 ºC for 30 min, then the beads were collected by magnet and resuspended in 20 µl ThermoPol reaction mix (1X ThermoPol buffer, 1 µl RppH, 1 µl RiboLock RNAse inhibitor), then incubated at 37 ºC for 1 hr. Beads were once again collected by magnet, then the 5' RNA adaptor (REV5) was ligated using T4 RNA ligase, setting up the reaction using the provided manual and incubating at 25 ºC for 1 hr. Beads were then washed once with high salt wash buffer, transferring to a clean tube, then once with low salt buffer, before being resuspended in 300 µl of TRIzol reagent (Ambion). Samples were vortexed for 20 sec, then incubated on ice for 3 min before adding 60 µl of chloroform, vortexing for 15 sec, then incubating on ice for a further 3 min. Samples were then spun at 20,000 x *g* for 8 min at 4 ºC, then the upper ~180 µl aqueous phase was transferred to a clean tube and precipitated using a standard ethanol precipitation.

Finally, pellets were resuspended in 13.5 µl reverse transcription resuspension mix (8.5 µl DEPC water, 4 µl 10 µM primer RP1, 1 µl 10 mM dNTPs), denaturing at 65 ºC for 5 min, snap cooling on ice. Reverse transcription was then performed using Maxima H Minus RT (Thermo Fisher Cat. No. EP0753) by adding 6.5 µl RT master mix (4 µl 5X RT buffer, 1 µl DEPC water, 0.5 µl RiboLick RNAse inhibitor, 1 µl Maxima H Minus RT), then cycling as follows: 50 ºC for 30 min, 65 ºC for 15 min, 85 ºC for 5 min. 2.5 µl of indexed RPI-n primer (10 µM) were then added to each RT reaction, then PCR was performed as a 100 µl reaction

using the Q5 polymerase (NEB) with the included high GC content enhancer. Samples were then PCR-amplified to the beginning of the logarithmic phase, as determined using a small-scale qPCR reaction run in parallel (typically less than 20 cycles).

Libraries were sequenced as described previously at the Vienna BioCenter Core Facilities Next Generation Sequencing Core. The data analysis was performed by adapting available pipelines.[82] Briefly, we created a Nextflow container (URL/Github) to perform all QC, alignment, and read processing steps, generating strand-specific bigwig files that were subsequently analyzed in R.

ChIP-qPCR

S. pombe (100 ml) were grown to mid-exponential phase (OD_{600} ~0.4-0.5) in YES, fixed with 1% formaldehyde for 15 min, quenched with 125 mM glycine for 10 min, then collected by centrifugation. Cells were washed once with ice-cold PBS, then resuspended in lysis buffer (50 mM HEPES-KOH, pH 7.5, 140 mM NaCl, 1 mM EDTA, 0.1% sodium deoxycholate, 0.1% Triton X-100, 1X Roche Complete Protease Inhibitors), and then lysed using acid-washed glass beads in a Precellys for four rounds 20 sec maximum speed, 1 min on ice. Lysate was then separated from the beads and then chromatin was sheared to a predominant final DNA length of ~150-200 bp in a Covaris E220 ultrasonicator, and then clarified of unlysed cells and debris by centrifugation twice at 20,000 × *g* for 10 min. Prepared chromatin was then frozen at -70 ºC pending use.

Chromatin aliquots were thawed on ice, then normalized based on starting culture density using additional lysis buffer for dilution. 10% of normalized and diluted chromatin were reserved as input controls. Anti-H2A.Z(Pht1) antibody (2µg) was then added to each culture and samples were incubated overnight at 4 ºC with inversion. 25 µl of Protein A Dynabeads (Thermo Fisher Cat. No. 10001D) per sample were prepared by washing twice with

PBS with 0.1% tween-20, once with lysis buffer, then resuspending in 50 µl of lysis buffer. Prepared beads were then combined with overnight chromatin samples, and incubated for 4 hrs at 4 ºC with inversion. Beads were then collected using the magnet and washed twice with lysis buffer, twice with high salt lysis buffer (50 mM HEPES-KOH, pH 7.5, 500 mM NaCl, 1 mM EDTA, 0.1% sodium deoxycholate, 0.1% Triton X-100), twice using lithium wash buffer (10 mM Tris-HCl, pH 8, 250 mM LiCl, 1 mM EDTA, 0.5% NP-40, 0.5% sodium deoxycholate), and once with TE. Beads were then resuspended in 100 µl of elution buffer (50 mM Tris-HCl, pH 8, 10 mM EDTA, 0.8% SDS) and transferred to PCR strips. Samples were then boiled for 10 min at 95 ºC, then 65 ºC overnight in a thermocycler. The next morning, proteinase K was added (final concentration 0.2 mg/mL) and incubated at 55 °C for 1 h. Samples were then cleaned up using a commercial kit (Zymo Research Cat. No. D5201). DNA concentration was measured by Nanodrop spectrophotometer. To verify the H2A.Z antibody, ChIP-qPCR was set up as previously described, with samples being diluted 100-fold.

Quantification and Statistical Analysis

Unless otherwise noted, all statistical analyses were performed in R (v4.1.3) using the RStudio IDE (v2022.12.0+353) on x86_64-apple-darwin17.0 (64-bit) under macOS 13.6.3. All statistical tests used are stated in corresponding figure legends. Quantification of sequence distances was performed using CLC Main Workbench 10 (Qiagen). Processing of NGS data, as well as all AlphaFold2 Multimer analyses, were performed using the CLIP cluster (https://clip.science).

Data, Code, and Materials Availability

PRO-seq pipeline and scripts used for data analysis are available as a container on Github, and all other scripts used in analysis are available upon request to the lead contact.

NGS data (PRO-seq, mRNA-seq) are deposited in GEO under accession number GSE265749 and GSE265775, respectively. For material request (e.g. strains), please contact the lead (zachary.harvey@gmi.oeaw.ac.at).

References

1. Luger, K., Mader, A.W., Richmond, R.K., Sargent, D.F., and Richmond, T.J. (1997). Crystal structure of the nucleosome core particle at 2.8 A resolution. Nature *389*, 251-260. 10.1038/38444.

2. Meneghini, M.D., Wu, M., and Madhani, H.D. (2003). Conserved histone variant H2A.Z protects euchromatin from the ectopic spread of silent heterochromatin. Cell *112*, 725-736. 10.1016/s0092-8674(03)00123-5.

3. Allis, C.D., Richman, R., Gorovsky, M.A., Ziegler, Y.S., Touchstone, B., Bradley, W.A., and Cook, R.G. (1986). hv1 is an evolutionarily conserved H2A variant that is preferentially associated with active genes. Journal of Biological Chemistry *261*, 1941-1948. 10.1016/s0021-9258(17)36034-9.

4. Yelagandula, R., Stroud, H., Holec, S., Zhou, K., Feng, S., Zhong, X., Muthurajan, U.M., Nie, X., Kawashima, T., Groth, M., et al. (2014). The histone variant H2A.W defines heterochromatin and promotes chromatin condensation in Arabidopsis. Cell *158*, 98-109. 10.1016/j.cell.2014.06.006.

5. Costanzi, C., and Pehrson, J.R. (1998). Histone macroH2A1 is concentrated in the inactive X chromosome of female mammals. Nature *393*, 599-601. 10.1038/31275.

6. Giaimo, B.D., Ferrante, F., Herchenrother, A., Hake, S.B., and Borggrefe, T. (2019). The histone variant H2A.Z in gene regulation. Epigenetics Chromatin *12*, 37. 10.1186/s13072-019-0274-9.

7. Turinetto, V., and Giachino, C. (2015). Multiple facets of histone variant H2AX: a DNA double-strand-break marker with several biological functions. Nucleic Acids Res *43*, 2489-2498. 10.1093/nar/gkv061.

8. Perino, M., and Veenstra, G.J. (2016). Chromatin Control of Developmental Dynamics and Plasticity. Dev Cell *38*, 610-620. 10.1016/j.devcel.2016.08.004.

9. Valencia, A.M., and Kadoch, C. (2019). Chromatin regulatory mechanisms and therapeutic opportunities in cancer. Nat Cell Biol *21*, 152-161. 10.1038/s41556-018-0258-1.

10. Weiner, A., Hsieh, T.H., Appleboim, A., Chen, H.V., Rahat, A., Amit, I., Rando, O.J., and Friedman, N. (2015). High-resolution chromatin dynamics during a yeast stress response. Mol Cell *58*, 371-386. 10.1016/j.molcel.2015.02.002.

11. Wasylyk, B., Thevenin, G., Oudet, P., and Chambon, P. (1979). Transcription of in vitro assembled chromatin by Escherichia coli RNA polymerase. J Mol Biol *128*, 411-440. 10.1016/0022-2836(79)90095-0.

12. Tremethick, D., Zucker, K., and Worcel, A. (1990). The transcription complex of the 5 S RNA gene, but not transcription factor IIIA alone, prevents nucleosomal repression of transcription. J Biol Chem *265*, 5014-5023.

13. Almouzni, G., Mechali, M., and Wolffe, A.P. (1991). Transcription complex disruption caused by a transition in chromatin structure. Mol Cell Biol *11*, 655-665. 10.1128/mcb.11.2.655-665.1991.

14. Hirschhorn, J.N., Brown, S.A., Clark, C.D., and Winston, F. (1992). Evidence that SNF2/SWI2 and SNF5 activate transcription in yeast by altering chromatin structure. Genes Dev *6*, 2288-2298. 10.1101/gad.6.12a.2288.

15. Kulaeva, O.I., Hsieh, F.K., Chang, H.W., Luse, D.S., and Studitsky, V.M. (2013). Mechanism of transcription through a nucleosome by RNA polymerase II. Biochim Biophys Acta *1829*, 76-83. 10.1016/j.bbagrm.2012.08.015.

16. Nock, A., Ascano, J.M., Barrero, M.J., and Malik, S. (2012). Mediator-regulated transcription through the +1 nucleosome. Mol Cell *48*, 837-848. 10.1016/j.molcel.2012.10.009.

17. Clark-Adams, C.D., Norris, D., Osley, M.A., Fassler, J.S., and Winston, F. (1988). Changes in histone gene dosage alter transcription in yeast. Genes Dev *2*, 150-159. 10.1101/gad.2.2.150.

18. Knezetic, J.A., and Luse, D.S. (1986). The presence of nucleosomes on a DNA template prevents initiation by RNA polymerase II in vitro. Cell *45*, 95-104. 10.1016/0092-8674(86)90541-6.

19. Lorch, Y., LaPointe, J.W., and Kornberg, R.D. (1987). Nucleosomes inhibit the initiation of transcription but allow chain elongation with the displacement of histones. Cell *49*, 203-210. 10.1016/0092-8674(87)90561-7.

20. Cairns, B.R. (2009). The logic of chromatin architecture and remodelling at promoters. Nature *461*, 193-198. 10.1038/nature08450.

21. Yuan, G.C., Liu, Y.J., Dion, M.F., Slack, M.D., Wu, L.F., Altschuler, S.J., and Rando, O.J. (2005). Genome-scale identification of nucleosome positions in S. cerevisiae. Science *309*, 626-630. 10.1126/science.1112178.

22. Wang, H., Schilbach, S., Ninov, M., Urlaub, H., and Cramer, P. (2023). Structures of transcription preinitiation complex engaged with the +1 nucleosome. Nat Struct Mol Biol *30*, 226-232. 10.1038/s41594-022-00865-w.

23. Core, L., and Adelman, K. (2019). Promoter-proximal pausing of RNA polymerase II: a nexus of gene regulation. Genes Dev *33*, 960-982. 10.1101/gad.325142.119.

24. Jiang, D., and Berger, F. (2023). Variation is important: Warranting chromatin function and dynamics by histone variants. Curr Opin Plant Biol *75*, 102408. 10.1016/j.pbi.2023.102408.

25. Jiang, D., Borg, M., Lorkovic, Z.J., Montgomery, S.A., Osakabe, A., Yelagandula, R., Axelsson, E., and Berger, F. (2020). The evolution and functional divergence of the histone H2B family in plants. PLoS Genet *16*, e1008964. 10.1371/journal.pgen.1008964.

26. Herchenrother, A., Wunderlich, T.M., Lan, J., and Hake, S.B. (2023). Spotlight on histone H2A variants: From B to X to Z. Semin Cell Dev Biol *135*, 3-12. 10.1016/j.semcdb.2022.03.025.

27. Zhang, H., Roberts, D.N., and Cairns, B.R. (2005). Genome-wide dynamics of Htz1, a histone H2A variant that poises repressed/basal promoters for activation through histone loss. Cell *123*, 219-231. 10.1016/j.cell.2005.08.036.

28. Guillemette, B., Bataille, A.R., Gevry, N., Adam, M., Blanchette, M., Robert, F., and Gaudreau, L. (2005). Variant histone H2A.Z is globally localized to the promoters of inactive yeast genes and regulates nucleosome positioning. PLoS Biol *3*, e384. 10.1371/journal.pbio.0030384.

29. Raisner, R.M., Hartley, P.D., Meneghini, M.D., Bao, M.Z., Liu, C.L., Schreiber, S.L., Rando, O.J., and Madhani, H.D. (2005). Histone variant H2A.Z marks the 5' ends of both active and inactive genes in euchromatin. Cell *123*, 233-248. 10.1016/j.cell.2005.10.002.

30. Barski, A., Cuddapah, S., Cui, K., Roh, T.Y., Schones, D.E., Wang, Z., Wei, G., Chepelev, I., and Zhao, K. (2007). High-resolution profiling of histone methylations in the human genome. Cell *129*, 823-837. 10.1016/j.cell.2007.05.009.

31. Zilberman, D., Coleman-Derr, D., Ballinger, T., and Henikoff, S. (2008). Histone H2A.Z and DNA methylation are mutually antagonistic chromatin marks. Nature *456*, 125-129. 10.1038/nature07324.

32. Mavrich, T.N., Jiang, C., Ioshikhes, I.P., Li, X., Venters, B.J., Zanton, S.J., Tomsho, L.P., Qi, J., Glaser, R.L., Schuster, S.C., et al. (2008). Nucleosome organization in the Drosophila genome. Nature *453*, 358-362. 10.1038/nature06929.

33. Allis, C.D., Glover, C.V., Bowen, J.K., and Gorovsky, M.A. (1980). Histone variants specific to the transcriptionally active, amitotically dividing macronucleus of the unicellular eucaryote, Tetrahymena thermophila. Cell *20*, 609-617. 10.1016/0092-8674(80)90307-4.

34. West, M.H., and Bonner, W.M. (1980). Histone 2A, a heteromorphous family of eight protein species. Biochemistry *19*, 3238-3245. 10.1021/bi00555a022.

35. Malik, H.S., and Henikoff, S. (2003). Phylogenomics of the nucleosome. Nat Struct Biol *10*, 882-891. 10.1038/nsb996.

36. Liu, X., Bowen, J., and Gorovsky, M.A. (1996). Either of the major H2A genes but not an evolutionarily conserved H2A.F/Z variant of Tetrahymena thermophila can function as the sole H2A gene in the yeast Saccharomyces cerevisiae. Mol Cell Biol *16*, 2878-2887. 10.1128/mcb.16.6.2878.

37. Faast, R., Thonglairoam, V., Schulz, T.C., Beall, J., Wells, J.R.E., Taylor, H., Matthaei, K., Rathjen, P.D., Tremethick, D.J., and Lyons, I. (2001). Histone variant H2A.Z is required for early mammalian development. Current Biology *11*, 1183-1187. 10.1016/s0960-9822(01)00329-3.

38. Clarkson, M.J., Wells, J.R., Gibson, F., Saint, R., and Tremethick, D.J. (1999). Regions of variant histone His2AvD required for Drosophila development. Nature *399*, 694-697. 10.1038/21436.

39. Osakabe, A., Lorkovic, Z.J., Kobayashi, W., Tachiwana, H., Yelagandula, R., Kurumizaka, H., and Berger, F. (2018). Histone H2A variants confer specific properties to nucleosomes and impact on chromatin accessibility. Nucleic Acids Res *46*, 7675-7685. 10.1093/nar/gky540.

40. Horikoshi, N., Kujirai, T., Sato, K., Kimura, H., and Kurumizaka, H. (2019). Structure-based design of an H2A.Z.1 mutant stabilizing a nucleosome in vitro and in vivo. Biochem Biophys Res Commun *515*, 719-724. 10.1016/j.bbrc.2019.06.012.

41. Weber, C.M., Ramachandran, S., and Henikoff, S. (2014). Nucleosomes are context-specific, H2A.Z-modulated barriers to RNA polymerase. Mol Cell *53*, 819-830. 10.1016/j.molcel.2014.02.014.

42. Wen, Z., Zhang, L., Ruan, H., and Li, G. (2020). Histone variant H2A.Z regulates nucleosome unwrapping and CTCF binding in mouse ES cells. Nucleic Acids Res *48*, 5939-5952. 10.1093/nar/gkaa360.

43. Adam, M., Robert, F., Larochelle, M., and Gaudreau, L. (2001). H2A.Z is required for global chromatin integrity and for recruitment of RNA polymerase II under specific conditions. Mol Cell Biol *21*, 6270-6279. 10.1128/MCB.21.18.6270-6279.2001.

44. Santisteban, M.S., Kalashnikova, T., and Smith, M.M. (2000). Histone H2A.Z Regulates Transcription and Is Partially Redundant with Nucleosome Remodeling Complexes. Cell *103*, 411-422. 10.1016/s0092-8674(00)00133-1.

45. Santisteban, M.S., Hang, M., and Smith, M.M. (2011). Histone variant H2A.Z and RNA polymerase II transcription elongation. Mol Cell Biol *31*, 1848-1860. 10.1128/MCB.01346-10.

46. Stargell, L.A., Bowen, J., Dadd, C.A., Dedon, P.C., Davis, M., Cook, R.G., Allis, C.D., and Gorovsky, M.A. (1993). Temporal and spatial association of histone H2A variant hv1 with transcriptionally competent chromatin during nuclear development in Tetrahymena thermophila. Genes Dev *7*, 2641-2651. 10.1101/gad.7.12b.2641.

47. Mylonas, C., Lee, C., Auld, A.L., Cisse, II, and Boyer, L.A. (2021). A dual role for H2A.Z.1 in modulating the dynamics of RNA polymerase II initiation and elongation. Nat Struct Mol Biol *28*, 435-442. 10.1038/s41594-021-00589-3.

48. Allis, C.D., Ziegler, Y.S., Gorovsky, M.A., and Olmsted, J.B. (1982). A conserved histone variant enriched in nucleoli of mammalian cells. Cell *31*, 131-136. 10.1016/0092-8674(82)90412-3.

49. Coleman-Derr, D., and Zilberman, D. (2012). Deposition of histone variant H2A.Z within gene bodies regulates responsive genes. PLoS Genet *8*, e1002988. 10.1371/journal.pgen.1002988.

50. Berta, D.G., Kuisma, H., Välimäki, N., Räisänen, M., Jäntti, M., Pasanen, A., Karhu, A., Kaukomaa, J., Taira, A., Cajuso, T., et al. (2021). Deficient H2A.Z deposition is associated with genesis of uterine leiomyoma. Nature. 10.1038/s41586-021-03747-1.

51. Carter, B., Bishop, B., Ho, K.K., Huang, R., Jia, W., Zhang, H., Pascuzzi, P.E., Deal, R.B., and Ogas, J. (2018). The Chromatin Remodelers PKL and PIE1 Act in an Epigenetic Pathway That Determines H3K27me3 Homeostasis in Arabidopsis. Plant Cell *30*, 1337-1352. 10.1105/tpc.17.00867.

52. Jamge, B., Lorkovic, Z.J., Axelsson, E., Osakabe, A., Shukla, V., Yelagandula, R., Akimcheva, S., Kuehn, A.L., and Berger, F. (2023). Histone variants shape chromatin states in Arabidopsis. Elife *12*. 10.7554/eLife.87714.

53. Thakar, A., Gupta, P., McAllister, W.T., and Zlatanova, J. (2010). Histone variant H2A.Z inhibits transcription in reconstituted nucleosomes. Biochemistry *49*, 4018-4026. 10.1021/bi1001618.

54. Talbert, P.B., Ahmad, K., Almouzni, G., Ausio, J., Berger, F., Bhalla, P.L., Bonner, W.M., Cande, W.Z., Chadwick, B.P., Chan, S.W., et al. (2012). A unified phylogeny-based nomenclature for histone variants. Epigenetics Chromatin *5*, 7. 10.1186/1756-8935-5-7.

55. Dalmasso, M.C., Sullivan, W.J., Jr., and Angel, S.O. (2011). Canonical and variant histones of protozoan parasites. Front Biosci (Landmark Ed) *16*, 2086-2105. 10.2741/3841.

56. Heitman, J., Movva, N.R., and Hall, M.N. (1991). Targets for cell cycle arrest by the immunosuppressant rapamycin in yeast. Science *253*, 905-909. 10.1126/science.1715094.

57. Chernoff, Y.O., Lindquist, S.L., Ono, B., Inge-Vechtomov, S.G., and Liebman, S.W. (1995). Role of the chaperone protein Hsp104 in propagation of the yeast prion-like factor [psi+]. Science *268*, 880-884. 10.1126/science.7754373.

58. Crowley, P.D., and Gallagher, H.C. (2014). Clotrimazole as a pharmaceutical: past, present and future. J Appl Microbiol *117*, 611-617. 10.1111/jam.12554.

59. Samakkarn, W., Ratanakhanokchai, K., and Soontorngun, N. (2021). Reprogramming of the Ethanol Stress Response in Saccharomyces cerevisiae by the Transcription Factor Znf1 and Its Effect on the Biosynthesis of Glycerol and Ethanol. Appl Environ Microbiol *87*, e0058821. 10.1128/AEM.00588-21.

60. Yang, F., Kemp, C.J., and Henikoff, S. (2013). Doxorubicin enhances nucleosome turnover around promoters. Curr Biol *23*, 782-787. 10.1016/j.cub.2013.03.043.

61. Hoyos-Manchado, R., Reyes-Martin, F., Rallis, C., Gamero-Estevez, E., Rodriguez-Gomez, P., Quintero-Blanco, J., Bahler, J., Jimenez, J., and Tallada, V.A. (2017). RNA metabolism is the primary target of formamide in vivo. Scientific reports *7*, 15895. 10.1038/s41598-017-16291-8.

62. Torres-Garcia, S., Yaseen, I., Shukla, M., Audergon, P., White, S.A., Pidoux, A.L., and Allshire, R.C. (2020). Epigenetic gene silencing by heterochromatin primes fungal resistance. Nature *585*, 453-458. 10.1038/s41586-020-2706-x.

63. Suto, R.K., Clarkson, M.J., Tremethick, D.J., and Luger, K. (2000). Crystal structure of a nucleosome core particle containing the variant histone H2A.Z. Nat Struct Biol *7*, 1121-1124. 10.1038/81971.

64. Ehara, H., Kujirai, T., Shirouzu, M., Kurumizaka, H., and Sekine, S.I. (2022). Structural basis of nucleosome disassembly and reassembly by RNAPII elongation complex with FACT. Science *377*, eabp9466. 10.1126/science.abp9466.

65. Kujirai, T., Ehara, H., Fujino, Y., Shirouzu, M., Sekine, S.I., and Kurumizaka, H. (2018). Structural basis of the nucleosome transition during RNA polymerase II passage. Science *362*, 595-598. 10.1126/science.aau9904.

66. Stevens, K.M., Swadling, J.B., Hocher, A., Bang, C., Gribaldo, S., Schmitz, R.A., and Warnecke, T. (2020). Histone variants in archaea and the evolution of combinatorial chromatin complexity. Proceedings of the National Academy of Sciences *117*, 33384-33395. 10.1073/pnas.2007056117.

67. Jumper, J., Evans, R., Pritzel, A., Green, T., Figurnov, M., Ronneberger, O., Tunyasuvunakool, K., Bates, R., Zidek, A., Potapenko, A., et al. (2021). Highly accurate protein structure prediction with AlphaFold. Nature *596*, 583-589. 10.1038/s41586-021-03819-2.

68. Harris, M.A., Rutherford, K.M., Hayles, J., Lock, A., Bahler, J., Oliver, S.G., Mata, J., and Wood, V. (2022). Fission stories: using PomBase to understand Schizosaccharomyces pombe biology. Genetics *220*. 10.1093/genetics/iyab222.

69. The Gene Ontology, C. (2019). The Gene Ontology Resource: 20 years and still GOing strong. Nucleic Acids Res *47*, D330-D338. 10.1093/nar/gky1055.

70. Narain, A., Bhandare, P., Adhikari, B., Backes, S., Eilers, M., Dolken, L., Schlosser, A., Erhard, F., Baluapuri, A., and Wolf, E. (2021). Targeted protein degradation reveals a direct role of SPT6 in RNAPII elongation and termination. Mol Cell *81*, 3110-3127 e3114. 10.1016/j.molcel.2021.06.016.

71. Zumer, K., Maier, K.C., Farnung, L., Jaeger, M.G., Rus, P., Winter, G., and Cramer, P. (2021). Two distinct mechanisms of RNA polymerase II elongation stimulation in vivo. Mol Cell *81*, 3096-3109 e3098. 10.1016/j.molcel.2021.05.028.

72. Bortvin, A., and Winston, F. (1996). Evidence that Spt6p controls chromatin structure by a direct interaction with histones. Science *272*, 1473-1476. 10.1126/science.272.5267.1473.

73. McDonald, S.M., Close, D., Xin, H., Formosa, T., and Hill, C.P. (2010). Structure and biological importance of the Spn1-Spt6 interaction, and its regulatory role in nucleosome binding. Mol Cell *40*, 725-735. 10.1016/j.molcel.2010.11.014.

74. Adkins, M.W., and Tyler, J.K. (2006). Transcriptional activators are dispensable for transcription in the absence of Spt6-mediated chromatin reassembly of promoter regions. Molecular cell *21*, 405-416. 10.1016/j.molcel.2005.12.010.

75. Jeronimo, C., Watanabe, S., Kaplan, C.D., Peterson, C.L., and Robert, F. (2015). The Histone Chaperones FACT and Spt6 Restrict H2A.Z from Intragenic Locations. Mol Cell *58*, 1113-1123. 10.1016/j.molcel.2015.03.030.

76. Hong, J., Feng, H., Wang, F., Ranjan, A., Chen, J., Jiang, J., Ghirlando, R., Xiao, T.S., Wu, C., and Bai, Y. (2014). The catalytic subunit of the SWR1 remodeler is a histone chaperone for the H2A.Z-H2B dimer. Mol Cell *53*, 498-505. 10.1016/j.molcel.2014.01.010.

77. Close, D., Johnson, S.J., Sdano, M.A., McDonald, S.M., Robinson, H., Formosa, T., and Hill, C.P. (2011). Crystal structures of the S. cerevisiae Spt6 core and C-terminal tandem SH2 domain. J Mol Biol *408*, 697-713. 10.1016/j.jmb.2011.03.002.

78. Wu, W.H., Alami, S., Luk, E., Wu, C.H., Sen, S., Mizuguchi, G., Wei, D., and Wu, C. (2005). Swc2 is a widely conserved H2AZ-binding module essential for ATP-dependent histone exchange. Nat Struct Mol Biol *12*, 1064-1071. 10.1038/nsmb1023.

79. Luk, E., Ranjan, A., Fitzgerald, P.C., Mizuguchi, G., Huang, Y., Wei, D., and Wu, C. (2010). Stepwise histone replacement by SWR1 requires dual activation with histone H2A.Z and canonical nucleosome. Cell *143*, 725-736. 10.1016/j.cell.2010.10.019.

80. Shaw, R.J., Wilson, J.L., Smith, K.T., and Reines, D. (2001). Regulation of an IMP dehydrogenase gene and its overexpression in drug-sensitive transcription elongation mutants of yeast. J Biol Chem *276*, 32905-32916. 10.1074/jbc.M105075200.

81. Booth, G.T., Wang, I.X., Cheung, V.G., and Lis, J.T. (2016). Divergence of a conserved elongation factor and transcription regulation in budding and fission yeast. Genome Res *26*, 799-811. 10.1101/gr.204578.116.

82. Judd, J., Wojenski, L.A., Wainman, L.M., Tippens, N.D., Rice, E.J., Dziubek, A., Villafano, G.J., Wissink, E.M., Versluis, P., Bagepalli, L., et al. (2020). A rapid, sensitive, scalable method for Precision Run-On sequencing (PRO-seq). bioRxiv. 10.1101/2020.05.18.102277.

83. Vos, S.M., Farnung, L., Boehning, M., Wigge, C., Linden, A., Urlaub, H., and Cramer, P. (2018). Structure of activated transcription complex Pol II-DSIF-PAF-SPT6. Nature *560*, 607-612. 10.1038/s41586-018-0440-4.

84. Su, B.G., and Vos, S.M. (2024). Distinct negative elongation factor conformations regulate RNA polymerase II promoter-proximal pausing. Mol Cell. 10.1016/j.molcel.2024.01.023.

85. Bonisch, C., and Hake, S.B. (2012). Histone H2A variants in nucleosomes and chromatin: more or less stable? Nucleic Acids Res *40*, 10719-10741. 10.1093/nar/gks865.

86. Chakravarthy, S., Bao, Y., Roberts, V.A., Tremethick, D., and Luger, K. (2004). Structural characterization of histone H2A variants. Cold Spring Harb Symp Quant Biol *69*, 227-234. 10.1101/sqb.2004.69.227.

87. Arimura, Y., Kimura, H., Oda, T., Sato, K., Osakabe, A., Tachiwana, H., Sato, Y., Kinugasa, Y., Ikura, T., Sugiyama, M., et al. (2013). Structural basis of a nucleosome containing histone H2A.B/H2A.Bbd that transiently associates with reorganized chromatin. Scientific reports *3*, 3510. 10.1038/srep03510.

88. Horikoshi, N., Arimura, Y., Taguchi, H., and Kurumizaka, H. (2016). Crystal structures of heterotypic nucleosomes containing histones H2A.Z and H2A. Open Biol *6*. 10.1098/rsob.160127.

89. Kohestani, H., and Wereszczynski, J. (2021). Effects of H2A.B incorporation on nucleosome structures and dynamics. Biophys J *120*, 1498-1509. 10.1016/j.bpj.2021.01.036.

90. Michael, A.K., Stoos, L., Crosby, P., Eggers, N., Nie, X.Y., Makasheva, K., Minnich, M., Healy, K.L., Weiss, J., Kempf, G., et al. (2023). Cooperation between bHLH transcription factors and histones for DNA access. Nature *619*, 385-393. 10.1038/s41586-023-06282-3.

91. Sanulli, S., Trnka, M.J., Dharmarajan, V., Tibble, R.W., Pascal, B.D., Burlingame, A.L., Griffin, P.R., Gross, J.D., and Narlikar, G.J. (2019). HP1 reshapes nucleosome core to promote phase separation of heterochromatin. Nature *575*, 390-394. 10.1038/s41586-019-1669-2.

92. Grau-Bove, X., Navarrete, C., Chiva, C., Pribasnig, T., Anto, M., Torruella, G., Galindo, L.J., Lang, B.F., Moreira, D., Lopez-Garcia, P., et al. (2022). A phylogenetic and proteomic reconstruction of eukaryotic chromatin evolution. Nat Ecol Evol *6*, 1007-1023. 10.1038/s41559-022-01771-6.

93. Eddy, S.R. (2011). Accelerated Profile HMM Searches. PLoS Comput Biol *7*, e1002195. 10.1371/journal.pcbi.1002195.

94. Draizen, E.J., Shaytan, A.K., Marino-Ramirez, L., Talbert, P.B., Landsman, D., and Panchenko, A.R. (2016). HistoneDB 2.0: a histone database with variants--an integrated resource to explore histones and their variants. Database (Oxford) *2016*. 10.1093/database/baw014.

95. Richter, D.J., Berney, C., Strassert, J.F.H., Poh, Y.-P., Herman, E.K., Muñoz-Gómez, S.A., Wideman, J.G., Burki, F., and de Vargas, C. (2022). EukProt: A database of genome-scale predicted proteins across the diversity of eukaryotes. Peer Community Journal *2*. 10.24072/pcjournal.173.

96. Katoh, K., and Standley, D.M. (2013). MAFFT multiple sequence alignment software version 7: improvements in performance and usability. Mol Biol Evol *30*, 772-780. 10.1093/molbev/mst010.

97. Darriba, D., Posada, D., Kozlov, A.M., Stamatakis, A., Morel, B., and Flouri, T. (2020). ModelTest-NG: A New and Scalable Tool for the Selection of DNA and Protein Evolutionary Models. Mol Biol Evol *37*, 291-294. 10.1093/molbev/msz189.

98. Kozlov, A.M., Darriba, D., Flouri, T., Morel, B., and Stamatakis, A. (2019). RAxML-NG: a fast, scalable and user-friendly tool for maximum likelihood phylogenetic inference. Bioinformatics *35*, 4453-4455. 10.1093/bioinformatics/btz305.

99. Letunic, I., and Bork, P. (2019). Interactive Tree Of Life (iTOL) v4: recent updates and new developments. Nucleic Acids Res *47*, W256-W259. 10.1093/nar/gkz239.

100. Maundrell, K. (1990). nmt1 of fission yeast. A highly transcribed gene completely repressed by thiamine. Journal of Biological Chemistry *265*, 10857-10864. 10.1016/s0021-9258(19)38525-4.

101. Yeast Extract with Supplements (YES). (2016). Cold Spring Harbor Protocols *2016*. 10.1101/pdb.rec091355.

102. Bahler, J., Wu, J.Q., Longtine, M.S., Shah, N.G., McKenzie, A., 3rd, Steever, A.B., Wach, A., Philippsen, P., and Pringle, J.R. (1998). Heterologous modules for efficient and versatile PCR-based gene targeting in Schizosaccharomyces pombe. Yeast *14*, 943-951. 10.1002/(SICI)1097-0061(199807)14:10<943::AID-YEA292>3.0.CO;2-Y.

103. Torres-Garcia, S., Di Pompeo, L., Eivers, L., Gaborieau, B., White, S.A., Pidoux, A.L., Kanigowska, P., Yaseen, I., Cai, Y., and Allshire, R.C. (2020). SpEDIT: A fast and efficient CRISPR/Cas9 method for fission yeast. Wellcome Open Res *5*, 274. 10.12688/wellcomeopenres.16405.1.

104. Murray, J.M., Watson, A.T., and Carr, A.M. (2016). Transformation of Schizosaccharomyces pombe: Lithium Acetate/ Dimethyl Sulfoxide Procedure. Cold Spring Harb Protoc *2016*, pdb prot090969. 10.1101/pdb.prot090969.

105. Gibson, D.G., Young, L., Chuang, R.Y., Venter, J.C., Hutchison, C.A., 3rd, and Smith, H.O. (2009). Enzymatic assembly of DNA molecules up to several hundred kilobases. Nat Methods *6*, 343-345. 10.1038/nmeth.1318.

106. DeAngelis, M.M., Wang, D.G., and Hawkins, T.L. (1995). Solid-phase reversible immobilization for the isolation of PCR products. Nucleic Acids Res *23*, 4742-4743. 10.1093/nar/23.22.4742.

107. Bray, N.L., Pimentel, H., Melsted, P., and Pachter, L. (2016). Near-optimal probabilistic RNA-seq quantification. Nat Biotechnol *34*, 525-527. 10.1038/nbt.3519.

108. Love, M.I., Huber, W., and Anders, S. (2014). Moderated estimation of fold change and dispersion for RNA-seq data with DESeq2. Genome Biol *15*, 550. 10.1186/s13059-014-0550-8.